Bioprinting alginate-gelatin soft biomaterial bioink for three-dimensional cancer cell culture.

Salvador Flores Torres

M. Eng Candidate

Bioengineering Department

Engineering Faculty

McGill University, Montreal

October 2018

Thesis supervisor: Joseph “Matt” Kinsella

A thesis submitted to McGill University in partial fulfillment of the requirements of the degree of Master on Engineering in Biological and Biomedical Engineering.

Table of Contents

List of abbreviations

2D	Two-dimensional
3D	Three-dimensional
A1G7	Alginate 1% and gelatin 7%
CAFs	Cancer associated fibroblasts
dECM	Decellularized extracellular matrix
ECM	Extracellular matrix
EndMT	Endothelial-mesenchymal transition
FN	Fibronectin
FTIR	Fourier-transform infrared spectroscopy
GM	Geometric mean
HT	high-throughput
LIFT	Laser-induced forward transfer
LOX	Lysyl oxidase
MCTSs	Multicellular tumor spheroids
PDGF	Platelet-derived growth factor
PGs	Proteoglycans
ROCK	Rho-associated kinase
SLA	Stereolithography
TAMs	Tumor-associated macrophages
TGFβ	Transforming growth factor β
TME	Tumor microenvironment
VEGF	Vascular endothelial growth factor

List of figures

List of tables

Abstract

Malignant neoplasms or cancer occurs when cells acquire genetic instability causing uncontrolled cell growth with the potential of invading healthy tissues around the body. Interrogating cancer biology has been an exhausting task for many scientists. Cancer research and drug discovery depend upon robust and clinically relevant models. Most of our experiments are based on traditional, two-dimensional (2D) cell models in which cells are grown on flat, non-representative environments. Although 2D cell-based experiments had been the pillar of many ground-breaking discoveries, cells naturally grow in a volumetric space to form soft tissues and organs structures along with a complex extracellular matrix (ECM) arrangement. Fundamental understanding of cancer cannot be fully concluded from 2D studies due to the lack of physiologically-relevant conditions such as cell-cell and cell-ECM interactions. In this work, we evaluate the use of a naturally-derived biomaterial as an ECM analog to perform 3D cancer cell culture for long periods of time (>80 days). We rely on extrusion bioprinting techniques to produce cancer cell-laden scaffolds with high-reproducibility and control over the initial conditions. This project aims to integrate both engineering approaches and biological principles to present a novel technique to apply biomaterials in cancer research.

Résumé

Les néoplasmes malins, ou tumeurs cancéreuses, surviennent lorsque les cellules acquièrent une instabilité génétique causant une croissance cellulaire incontrôlée ayant le potentiel d'envahir les tissus sains autour du corps. Les interrogations au sujet de la biologie du cancer ont été épuisante pour de nombreux scientifiques. La recherche sur le cancer et la découverte de médicaments dépendent de modèles solides et cliniquement pertinents. La plupart de nos expériences sont basées sur des modèles cellulaires bidimensionnels (2D) classiques, dans lesquels les cellules sont cultivées dans des environnements plats et non représentatifs. Bien que ces expériences en 2D aient été le pilier de nombreuses découvertes révolutionnaires, les cellules se développent naturellement dans un espace volumétrique pour former des structures de tissus mous et d'organes avec une matrice extracellulaire complexe (ECM). La compréhension fondamentale du cancer ne peut donc pas être entièrement conclue à partir d'études réalisées en 2D, car les conditions physiologiques telles que les interactions cellules-cellules et cellules-ECM manquent. Dans ce travail, nous évaluons l'utilisation d'un biomatériau d'origine naturelle comme analogue dECM pour réaliser des cultures de cellules cancéreuses en 3D pendant de longues périodes (>80 jours). Nous nous appuyons sur des techniques de bioimpression par extrusion pour produire des échafaudages chargés de cellules cancéreuses avec une grande reproductibilité et un fort contrôle des conditions initiales. Ce projet vise à intégrer à la fois des approches d'ingénierie et des principes biologiques pour présenter une nouvelle technique d'application des biomatériaux dans la recherche sur le cancer.

Acknowledgments

First and foremost, I would like to thank my supervisor Joseph “Matt” Kinsella from the Bioengineering Department at McGill University. His valuable support and guidance made me reach the goals of this project. Having the opportunity to be part of his laboratory has been a unique journey, full of professional and personal learning experiences.

I want to thank all the people that collaborated in this project: Dr. Veena Sangwan (McGill University) for providing the cells for this study. Her suggestions and help with the biological interpretations of my results; the outcome would not have been the same. Many thanks to Denis Flipo (Université du Quebéc à Montréal) for his guidance in microscopy and image acquisition. Also, special thanks to Cleber Silveira Moraes, Caroline Therien, and all the people from the histocore (Goodman Cancer Research Center) who performed the staining. Special thanks to my co-workers and friends Jacqueline Kort Mascort, Tao Jiang, Pooja Pushparaj, Jose Gil Munguia Lopez, Nikolaos Dimitriou, and Abdrahman Maky Sakho for their guidance and support throughout this work.

I would also like to thank my funding agencies: CONACyT-i2t2, The Canadian Foundation for Innovation, Townshend-Lamarre Family Foundation, NSERC and McGill University for providing the financial support for me and this project

Finally, I would like to thank God for giving me the tools to find my way through.

Author’s contributions: All the experimentation and thesis writing were performed by Mr. Salvador Flores Torres. Unpublished data is being prepared for publication by Tao Jiang *et al.* (October 01, 2018).

1 Introduction and literature review

For 2017, it was estimated that 206,000 new cancer cases and 80,000 deaths occurred in Canada. One out of two Canadians will develop cancer during their lifetime, and one in four will die from the disease[1]. Human cancer behavior can be very diverse from individual to individual; metastasis can occur rapidly within a year, or it could take many years for a tumor to invade other tissues[2]. While significant improvements have been made in early diagnosis and anticancer therapies, resulting in an overall decrease in cancer mortality, tumorigenesis, tumor growth, and metastasis will continue to be considered as very complex events to be studied *in vitro*. Although essential discoveries in cancer research and chemotherapeutics were done using traditional *in vitro* preclinical models such as monolayer cell culture and animal models, the likelihood of approval for a new drug from phase I clinical trials is still ~ 7%[3], suggesting the need for more relevant and robust preclinical models to perform pharmaceutical testing and biological research. Recent literature has shown that cancer formation, progression, and metastasis events are dependent upon the tumor microenvironment (TME) and it has been proven that the TME is responsible for promoting tumor resistance and recurrence[4]. These observations encouraged tissue engineering techniques to be implemented with the goal of recapitulating essential aspects of the TME as an *in vitro* preclinical model; hypothesizing that having control of the TME composition will allow identification of druggable targets within the TME, the development of new therapeutic strategies and novel research approaches.

1.1 Hypothesis

In this work, we hypothesize that having control of the TME initial conditions (biocomposition and dwelling cell types), malignant neoplastic phenomena can be recreated with high reproducibility and relevance. To test our hypothesis and control the initial conditions of TME, we propose the use of bioprinting techniques alongside novel biomaterials in the field, to engineer three-dimensional (3D) cancer cell-laden scaffolds.

1.2 The tumor microenvironment

Cancerous cells dwell and develop within a complex heterogeneous three-dimensional (3D) environment known as the tumor microenvironment (TME)[5]. The TME is extremely heterogeneous; known to be comprised of many cell populations and a structural extracellular matrix (ECM). Cells within the TME include fibroblasts, cancer-associated fibroblasts (CAFs), tumor-associated macrophages (TAMs), endothelial cells, immune cells, adipocytes, pericytes, mesenchymal cells, among others[6]. The cells that create the TME are usually non-malignant cells. However, these cells can have tumor-promoting functions throughout cancer development[7]. The stroma is an important constituent of the TME. CAFs are a predominant and multi-functional cell type of the tumor stroma. These cells are known to deposit ECM components and promote tumor progression; they regulate epithelial cell differentiation, immune responses, and homeostasis[8,9]. The following sections will review the TME components and their role in cancer progression.

1.2.1 The extracellular matrix

The extracellular matrix (ECM) is the non-cellular component of all tissues and organs. It is composed of a heterogeneous mixture of water, proteins, glycoproteins, and

proteoglycans, that provide not only structural stability but also promotes various biochemical signals to modulate cellular function[10,11]. The ECM physical and biochemical integrity are important for a wide range of diseases, including severe syndromes, that arise from abnormalities in ECM composition[12]. The ECM structure is continuously remodeled by enzymatic and non-enzymatic reactions; its components are subject to modifications driven by cells or external stimuli. Moreover, cell adhesion to the ECM is mediated by ECM binding sites that interact with transmembrane receptors of cells, such as integrins. Also, the ECM promotes the essential morphological organization and physiological functions of the cells by secreting growth factors and interacting with the cells to trigger signal transduction that regulates gene expression[13].

The primary molecular components of the ECM are proteoglycans (PGs) and fibrous proteins[12]. The main ECM proteins are collagens, elastins, fibronectins, and laminins. Collagen is the most abundant protein and the main structural element of the ECM; it regulates cell adhesion, supports events such as chemotaxis, cell migration, and tissue development, and accounts for the intrinsic tensile strength of tissues[14]. Collagen proteins are secreted in bulk format by fibroblasts that are present either in the stroma or surrounding tissues. Fibroblast influence the alignment of collagen fibers by reorganizing the collagen into different structures such as sheets and cables. These fibers are made up of a heterogeneous mix of different types of collagen, but usually, one type of collagen is predominant within the tissue (collagen I)[15,16]. Collagen also associates with other primary ECM fibers such as elastin. Elastin fibers provide elasticity that recoils tissues that undergo repeated stretching since it is approximately 1000 times more flexible than collagen. The precursor of the elastin (trophoblastic) is produced by fibroblasts, smooth

muscle cells, chondrocytes, or endothelial cells. Elastin monomers are formed by cleavage of its signal peptide to be finally enzymatically crosslinked by lysyl oxidase into elastin fibers[17].

Fibronectin, another fibrous protein of the ECM composition, it is involved in mediating cell attachments and functions. Fibronectin (FN) is considered a mechano-regulator as cells can stretch its structure to reveal additional and cryptic integrin binding sites within the length of the FN molecule. FN is involved in cell movement during development events, and it is also related to tumor metastasis[14].

The ECM is also a significant component of the TME and plays critical roles in progression. Uncontrolled ECM remodeling results in severe pathological complications and life threatening diseases[18]. Cells within the TME are known to deposit ECM components and change the ECM environment by stiffening and softening enzymatic processes[19]. The following section will elaborate on the cell types that reside in the TME and present of the concluding remarks and open questions in the literature.

1.2.2 Cells within the tumor microenvironment: Cancer-associated fibroblasts

The organizational framework that describes cellular properties during cancer progression were summarized as *"The Hallmarks of Cancer"* by Hanahan and Weinberg[20], and an update came a decade after their first publication[21]. In their revised work, Hanahan and Weinberg described the biological capabilities acquired during the development of human cancers. Within cancer, the TME tissue is composed of ECM and different cell types that orchestrate cancer development by undergoing phenotypic and genotypic changes. These unnatural modifications cause aberrant cell behavior and ECM

tissue modifications that influence or promote: genomic instability, angiogenesis, metastasis, tumor-promoting inflammation, aberrant division rates, immune evasion, evasion of growth suppressors, sustained proliferative signaling, cells resisting death, and deregulated cellular metabolism[21]. Cells within the TME include proliferating tumor cells, stromal cells, inflammatory cells and immune components, epithelial cells, endothelial cells, and many other tissue-associated cells. Among the cell types, the stromal components are known as cancer-associated fibroblasts (CAFs). These cells comprise approximately 50% of the cell types in cancers[22]. CAFs are a subpopulation of fibroblasts with a myofibroblastic phenotype present in cancer wounds[23]. Usually, myofibroblasts would be present during natural wound repair, however, unlike the natural wound healing process, CAFs produce tissue fibrosis[24].

Remarkably, a precise definition of CAFs is still under debate. Nonetheless, CAFs can be considered a cellular state rather than a cell type[25]. Moreover, another recent study hypothesizes that fibroblasts become activated during the initial stages of carcinogenesis, becoming CAFs that remodel the TME to start tissue repair and possibly, antitumoral functions. As the tumor progresses, these repair actions might promote further tumor growth. Evidence suggests that cancer cells might use CAF-secreted factors to facilitate tumorigenic activity[26-31]. Regardless of the CAF origin, research findings highlight factors that could activate CAFs within the milieu as: pH changes, low glucose and oxygen supply, unbalanced growth factors, cytokine up-down regulation, or mechanical changes within the TME[32,33] and the surrounding epithelial cells[34].

Furthermore, CAFs are known for their tumor-regulatory features. For instance, CAFs produce periostin, an ECM protein that is correlated with shorter survival and tumor growth[35]. Also, these cells are known to regulate cancer stem cells by secreting cytokines and growth factors[36]. Recent studies have reported that different kinds of cells could be recruited as CAFs with distinct functions: (1) resident tissue fibroblasts, (2) tumor-surrounding adipocytes, (3) mesenchymal stem cells derived from the bone marrow, (4) hematopoietic stem cells, (5) epithelial cells; through epithelial-mesenchymal transition (EMT), and (6) endothelial-mesenchymal transition (EndMT)[27,32,37-39]. Also, reported histochemical studies of human breast cancers have proven that tumor-infiltrating lymphocytes (TILs) were distributed next to CAFs, suggesting a close interaction between immune cells and CAFs[40]. Several studies showed that cells within the TME sustain a biomolecular dialogue with CAFS that favor tumorigenic behavior in the cells such as resistance to treatment[41] and metastasis[42].

Overall, cells within the TME play roles that promote cancer progression. When designing *in vitro* models to study neoplastic diseases, these cells and their specific functions should be considered. Accurate emulation of the TME can be accomplished by introducing such cells or their related by-products (growth factors or cytokines) by adding them to the cell nourishing media or the ECM analog composition.

1.2.3 Cancer metastasis and progression

Metastasis is a general description of the invasion events from the primary tumor site into surrounding healthy tissues and distant organs. It is estimated that cancer metastasis is responsible for 90% of cancer-related deaths[43]. The metastatic cascade involves a

sequentially-related series of events. Concisely, to complete the metastatic process, cancer-related cells must detach from the primary tumor site, enter the vascular or lymphatic systems, evade anti-tumoral immune attacks, exit the vascular or lymphatic systems at a distant site, and finally invade and proliferate in the healthy tissue[44-46]. Once it has occurred, the metastatic cells modify the microenvironment to facilitate angiogenesis for nutrient supply, resulting in a secondary malignant tumor. Numerous research groups make use of small animal models to study metastatic events. These approaches fail to provide relevant information since unnatural models of cancer invasion yield misleading information on the nature of the disease[47,48]. Growth, malignancy, and cancer progression are dynamic processes that involve many biological events. Therefore, the complexity and natural TME characteristics must be integrated when designing models to study neoplastic diseases. Currently, our pre-clinical models for cancer research and drug screening are limited because we rely on traditional 2D cell culture and animal models to predict clinical outcome. However, emerging technologies and recent research hypothesize that with a relevant biomaterial along with a useful technique to control the complexity of the 3D environment, *in vitro* TME recapitulation is possible. The following sections will introduce the current bioprinting techniques and their use in tissue engineering, along with the use of biomaterials and cell-laden bioinks to produce 3D cell culture methods.

1.3 Three-dimensional bioprinting: controlling the tumor microenvironment

The novel integration of bioprinting techniques and tissue engineering has become a common trend in many areas of clinical and biological research. By using bioprinting,

complex tissue microenvironments can be reproduced with enough accuracy to recapitulate physiological functions[49]. This engineering approach allows the use of multiple biomaterials and several cell types to create heterogeneous models while maintaining specific control over the position of these. Bioprinting techniques have been successfully implemented to produce biologically-relevant samples by using cell-laden biomaterials, commonly known as cell-laden bioinks. The main bioprinting techniques are inkjet, laser/light, and extrusion-based bioprinting[50].

1.3.1 Inkjet bioprinting

The inkjet technique was one of the first bioprinting methods to be developed. The working principle of this technique is to deposit the bioink in a droplet format; introducing small volume changes in the upper part of the nozzle that will generate a droplet ejection onto a platform[51]. Among many droplet generation mechanisms[52], the widely used ones are piezo-electric[53] and thermal induced bubble[54]. The main reasons to implement inkjet bioprinting, as well as the drawbacks of the technique, are shown in Table 1[55-61].

Table 1 Advantages and disadvantages of inkjet bioprinting techniques

Advantages	Disadvantages
Non-expensive technique	Bioink viscosity is limited to <15 mPa s. Limited cell density (usually <1x10^6 cells/mL)
Bioprinted models can be created at high speeds without compromising quality	Settling effects and aggregation within the bioink reservoir obstruct the nozzle and cause high heterogeneity of the final product.
Biological contamination is reduced due to the minimal contact between mechanical parts and the bioink.	The produced small droplets (pico-liter scale) are susceptible to drying. Cells are known to be affected by dehydration.

1.3.2 Stereolithography (laser/light)

Stereolithography (SLA) is a well developed rapid manufacturing technique that utilizes a reservoir filled with a photosensitive polymer solution. The working principle depends on a laser beam focus that is moved in 3D space (X, Y, Z directions) and cures the material within the reservoir as it moves from point to point. Using photo-curable polymer biomaterials or photosensitive proteins, SLA has become a feasible technique in tissue engineering. The main reasons to implement SLA bioprinting, as well as the drawbacks of the technique, are shown in Table 2[62-66].

Table 2 Advantages and disadvantages of stereolithography bioprinting techniques.

Advantages	Disadvantages
High resolution (down to several μm).	Bioinks are limited only to photosensitive biomaterials.
Pore size control due to the resolution level.	Photocuring can be detrimental to cells if ionizing energy is used (i.e. UV).
High-speed production can be achieved through the implementation of digital mirror devices.	Unable to work with different cell types due to the nature of the reservoir design.

1.3.3 Laser-induced forward transfer (laser/light)

Laser-induced forward transfer (LIFT) takes advantage of an energy absorbing material that responds to light stimulation. LIFT involves a laser beam, a focusing system, and a bilayer 'ribbon': a photosensitive donor layer (i.e. gold or titanium) and a layer of bioink material, usually suspended under the donor layer. The bioink deposition principle of LIFT depends on a laser beam that vaporizes a region of the donor layer, forming a bubble at the interface of both layers and the result is a droplet of bioink that is ejected towards the

building platform. The main reasons to implement LIFT bioprinting, as well as the drawbacks of the technique, are shown in Table 3[67-71].

Table 3 Advantages and disadvantages of laser-induced forward transfer bioprinting techniques.

Advantages	Disadvantages
Non-contact printing technique: reduced contamination and nozzle clogging.	Working with multiple may be non-feasible.
The technique manages a wide range of material viscosities (1-300 mPa s).	The generation of droplets is a randomized process, requiring a near-confluent cell-laden layer to ensure homogeneity.
High cell densities can be handled ($1x10^8$ cells/mL).	Expensive technique compared to the other ones.

1.3.4 Extrusion-based bioprinting

Extrusion-based bioprinting is the most common and affordable technique due to its simple mechanical setup. The bioink materials are filled into cartridges and extruded through a nozzle by either pneumatic pressure or mechanical force. Generally, the cartridges are mounted onto a mobile XYZ stage, and the pressure is controlled by a computer. Additional parameters such as temperature can also be tuned during the bioprinting process. The main reasons to implement extrusion-based bioprinting, as well as the drawbacks of the technique are shown in Table 4[72-80].

Table 4 Advantages and disadvantages of extrusion-based bioprinting techniques.

Advantages	Disadvantages
The technique allows high cell densities ($>1x10^6$) and a wide variety of bioink materials simultaneously.	Cell viability compromised if high pressures are used to extrude the cell-laden bioinks.

The temperature control allows tuning the bioink properties as well as physiological conditions during the extrusion process.	Many bioink materials exhibit viscoelastic properties that require rheological characterization to understand their behavior under shear stress conditions.
The technique allows the creation of heterogeneous models by using multiple cartridges loaded with different cells and bioinks.	Printing resolution and speed are not as high as other techniques.

This work relies on extrusion-based bioprinting since the technique allows customization and user- and cell-friendly operations. The following section will highlight the critical considerations when choosing a biomaterial for an ECM analog in cell culture applications.

1.4 Biomaterials as an in vitro cell niche

Current efforts in tissue engineering to recapitulate the native ECM environment have deserted traditional 2D cell culture on glass and plastic surfaces to favor relevant 3D culture systems, where cells are encapsulated and cultured inside biomaterial scaffolds. Bissell and coworkers[81] highlighted that examining biology in 2D is insufficient for conclusive results. Moreover, they showed that human breast epithelial cells develop and behave like tumors when cultured in 2D systems but show normal growth behaviors when cultured in 3D ECM analogs of their native microenvironment. As shown by Bissell and coworkers, the feasibility of the method relies on the attributes of the biomaterials; intrinsic ECM and TME components provide biochemical and mechanobiological stimuli to the cells in culture to promote native behaviors.

Polymers of natural or synthetic origin are widely used to provide ECM and TME analogs in 3D cell culture. ECM-mimicking polymers are known to increase the clinical relevance of the *in vitro* environment by giving a volumetric space that favors cell biochemical and

mechanical stimuli[82]. These biomaterials are usually manufactured or prepared in a gel, hydrogel, or hydrogel precursor form. Considering that native tissue is mostly composed of water, the most attractive characteristic of these biomaterials is their ability to entrap substantial amounts (>90%) of this vital liquid. The water content of these materials allows cells to be embedded and placed in their final culture environment without damage from dehydration[83]. However, since most of these materials possess poor mechanical properties, setting 3D culture environments by hand, results in heterogeneous non-reproducible environments due to the lack of control over essential parameters such as geometry, cell density, and cell position. Also, most of these polymeric hydrogel structures possess physical characteristics that are dynamic in time (temperature-dependent), reducing the handling time. To overcome these difficulties, current tissue engineering technologies have adopted the use of bioprinting techniques along with unique composite hydrogel biomaterials. Composite hydrogels can be tuned by blending different components to achieve specific biocompatible characteristics. Overall, the core of this project relies on the use of biomaterials to simulate native ECM and TME properties *in vitro.* The following section will introduce the concept of a bioink material for bioprinting applications, their biomechanical requirements, and some of their applications.

1.4.1 Bioink materials for extrusion-based bioprinting

A bioink material is defined as the material used in 3D bioprinting where cells, biological components, or combination of both are deposited in a volumetrically controlled pattern to fabricate living tissues and cell-laden scaffolds. The main purposes of the bioink material are: (1) provide post-printing structural support, (2) transport cells into the desired structure, and (3) sustain cell populations. Depending on the application, the

biodegradability of the matrix could be considered. Moreover, some natural bioink components from the native ECM can be used to promote cell adhesion sites, intrinsic cell morphology, and native cell behavior (differentiation and proliferation)[84]. However, some these native components contain countless biomolecules that contribute to a high heterogeneity of the final *in vitro* model. To simplify the bioink composition, bottom-up approaches are used to produce bioink formulations of one or two main components[85]. On the other hand, the top-down technique works with native decellularized extracellular matrix (dECM) or its components, from either healthy or diseased tissue to engineer 3D models[86]. Choosing between these approaches results in a trade-off between the physiological relevance, reproducibility of results, and the mechanical integrity of the final *in vitro* model.

The biochemical properties of the bioinks are dictated by the biological requirements of the embedded cells or tissues. These requirements can be satisfied either with natural or synthetic materials. For instance, if the 3D model of interest is intended to be used with anchoring dependent cells, ECM components that promote anchoring (collagen or gelatin) sites must be introduced into the bioink formulation. For the opposite scenario, in which cells require to be grown as aggregates or spheroids, a material with bioinert characteristics should be considered (i.e. alginate or agarose).

For tissue engineering and bioprinting applications, cell-laden hydrogels and cell-laden hydrogel precursors are used as bioinks to create tissue constructs. However, most of these materials exhibit viscoelastic properties such as shear-thinning, meaning that mechanical stress during the extrusion process changes the material physical attributes

while it flows through the cartridge nozzle. Popular biomaterials used in 3D bioprinting and their attributes are shown in Table 5.

Table 5 Popular hydrogel biomaterials used for bioink manufacturing

Material	Biological features	Mechanical features
Agarose	Naturally-derived polysaccharide. Does not provide adhesion sites. Requires biochemical modification to enhance biocompatibility[87].	Brittle material in its solid state. Maintains its shape for extended periods of time. Serves as a mold material for 3D cell culture[88].
Alginate	Naturally-derived polysaccharide. Proteins are minimally absorbed[89]. Requires biochemical modification to promote cell adhesion[90].	Superior mechanical properties can be achieved by crosslinking the material. Viscosity depends upon alginate concentration[91].
Chitosan	Naturally-derived linear polysaccharide. Exhibits hemostatic and antibacterial activity[92].	Unstable mechanical properties[93]. Requires crosslinkers to enhance mechanical properties[94].
Collagen type I	Naturally-derived triple helical protein[95]. Allows cell adhesion and growth[96]	Collagen fibrillogenesis is a thermally-dependent process, and the pH of the media impacts the stability of fibrillar structures[97].
Fibrin	Formed by an enzymatic reaction between thrombin and fibrinogen. Supports cell growth and proliferation. Not suitable for long-term cell culture as the fibrin degrades very fast[98,99].	Non-linear elasticity. Fibrin networks allow high deformations without breaking. Cannot be manipulated after gelation. Requires mechanical support to increase its bioprintability[100,101].
Gelatin	Denatured form of collagen protein. Less immunogenic than collagen. Promotes cell adhesion, differentiation, migration, and proliferation[102]. Allows long-term cell viability but low cell elongation[103,104].	Forms gel-like structures at low temperatures and reverts to liquid as temperature increases[105]. Requires crosslinking to maintain its shape in cell culture conditions.
Hyaluronic acid	Linear non-sulfated glycosaminoglycan. Offers high biocompatibility. Cell-	Slow gelation rate and poor mechanical properties. Requires

	mediated hydrogel degradation[98].	mechanical support or crosslinking to increase bioprintability[106].
GelMA	Denatured form of collagen chemically modified as a synthetic hydrogel. Offers low proliferation rates. Cell morphology and shape influenced by GelMA concentration[104].	High mechanical strength. Low swelling ratio. UV exposure time alters crosslinking rate[104].
Pluronic® F-127	Poloxamer-based compound. Cell viability is not possible to achieve for extended periods of time[107].	Undergoes reverse gelation as it cross-links with high temperatures and liquefies at low temperatures. Requires chemical modification to avoid rapid degradation[108].
Polyethylene glycol	Linear polyether hydrophilic compound[109]. Needs biochemical modification to offer cell adhesion components[110]. Some cell types can survive without any additives[111].	Poor mechanical strength. Requires mechanical support or crosslinking to increase bioprintability[84,112].

Blends of synthetic and natural polymers enhance the hydrogel biological and mechanical properties according to the application. Some other approaches have reported the use of nanoparticles to increase the biocompatibility and mechanical stability of the hydrogel bioink[113]. However, to retain the structural integrity of the bioprinted model *in vitro* conditions (cell culture media, 5% CO2, and 37°C), hydrogel precursor materials require post-printing crosslinking. The crosslinking process can either be by physical or chemical means. Physical approaches to perform crosslinking include the use of hydrophobic reactions, ionic interactions, and hydrogen bonding[84].

On the other hand, chemical crosslinking relies on the formation of covalent bonds (includes photo-crosslinking). The main difference between these approaches is that the chemical crosslinking forms stronger networks as compared to the physically crosslinked

hydrogels. Moreover, it is worth mentioning that some of the crosslinking methods may affect cell viability[84].

For this project, the use of a composite hydrogel comprised of alginate and gelatin is proposed. Alginate is naturally non-cell adhesive and requires either chemical modification or blending with other materials[114,115]. Furthermore, alginate crosslinking is possible in an aqueous solution of $CaCl_2$, and the de-crosslinking process can be carried out by soaking the alginate structure in an aqueous solution of sodium citrate[116]. Post-printing crosslinking ensures mechanical stability as the process increases the stiffness of the material and de-crosslinking allows the extraction of the encapsulated biological components. On the other hand, the gelatin component provides bioactivity to the blend, since it contains the linear RGD cell adhesive motif. The RGD is the most abundant peptide responsible for cell adhesion in ECM through integrin ligation[117].

The ability to tune the stiffness and bioactivity of the microenvironment by modifying the alginate and gelatin concentrations, allows us to mimic essential conditions of the TME in different cancer stages. For example, in tumors, cancer-associated fibroblasts (CAFs) are known to start a fibrotic response that leads to an accumulation of fibrillar ECM proteins, a condition known as a desmoplastic reaction[118]. Desmoplastic conditions can be simulated by increasing ECM components within the matrix and by co-culturing fibroblasts along with cancer cells[119].

Our laboratory has extensively characterized different alginate/gelatin bioink biological and mechanical attributes. The alginate concentration (1, 3, and 5 w/v %) was found to be inversely related to cell proliferation and survival, suggesting that high concentrations

of alginate could reduce viability for specific cell types. Moreover, regardless of the gelatin concentrations (5, 7, and 9 w/v%) considered for the study, the alginate concentration drove the cell behavior during the experiments; inversely related to viability and proliferation (unpublished data, Jiang *et al.* 2018). The bioink selection for this work is comprised of 1% alginate (w/v) and 7% gelatin (w/v) since it was one of the composite hydrogels that promoted cell development for extended periods of time.

2 Materials and methods

2.1 Bioink manufacturing

Hydrogel precursors were acquired in powder form; sodium alginate (Protanal LF 10/60 FT, FMC biopolymer) and Type B gelatin from bovine skin (G9391, Sigma-Aldrich) powders were sterilized via UV exposure for 6 h. Every 180 min, the powder was agitated to maximize the UV effect. The composition of the bioink was set to 1 w/v% of alginate and 7 w/v% of gelatin (A1G7). Both powders were dissolved in sterile DPBS (1x, w/o calcium, w/o magnesium, Gibco) and mixed using a magnetic hotplate for 1 h at 55 °C and then for 2 h at room temperature (24 °C). The final mixed hydrogel precursor was then transferred to sterile centrifuge tubes and centrifuged at 2,000 rpm for 10 minutes to eliminate bubbles. Finally, the centrifuged product was stored in a 4 °C fridge and used within one week.

The crosslinking solution was prepared by dissolving $CaCl_2$ (Sigma-Aldrich) into Milli Q water (100 mM). The de-crosslinking solution was prepared by dissolving sodium citrate (Sigma-Aldrich) into MilliQ water (55 mM). Both solutions were sterilized by filtering (0.22 µm pore). The final sterilized solutions were also stored in a 4 °C fridge until use. All material preparation was carried out with aseptic laboratory practices; inside a biosafety cabinet, using pre-sterilized utensils and glassware, protecting laboratory equipment, and pre-sterile storage containers.

2.2 Bioink physicochemical characterization

Before mixing the bioink with cells, characterization tests were performed to discard any biological contaminants (bacteria), ensure the optimal bioink gelation time, and confirm

the final composition of the hydrogel blend. These tests must be considered before using the bioink. Failure to do so could result in aberrant cell behavior and unfavorable mechanical properties during extrusion. The following sections will detail the bioink characterization before its application as a cell-laden scaffold.

2.3 Rheology: gelation kinetics

Rheological tests were conducted on an MCR302 rheometer (Anton Paar, Canada) with an Φ 25 mm parallel measuring tool (PP25). Our lab previously determined the amplitude sweeps. These were initially performed to measure the ultimate linear strain γ_c (determined as 1/10 of the ultimate linear strain, for safety reasons). The bioink was pre-heated in a water bath at 37 °C for 2 h to allow thermal stabilization of the material. The rheometer testing plate was pre-heated to 37 °C. The hydrogel precursors were loaded onto the plate of the rheometer, and the temperature was decreased from 37 °C to 20 °C at the start of the analysis. While the test was being performed, a sinusoidal strain of γ_c at 1 Hz was applied for a period of 2 h. G' and G'' were recorded once per minute during the gelation process. It is worth mentioning that pre-heating times of 30 min did not cause significant differences in the results.

2.4 Fourier-transform infrared spectroscopy (FTIR)

Chemical formulation of the hydrogel constituents and the post-printing structures were evaluated by an FTIR-ATR spectrometer (FTIR, Smart iTR, Thermo Scientific). The spectral window was set from 4000 to 500 cm-1. Alginate and gelatin were tested independently in their powder format. Each powder was placed to cover the area of the analysis crystal. The crosslinked A1G7 samples were freeze-dried for dehydration. Disk-

shaped samples were considered to cover the area of the analysis crystal. Data was recorded.

2.5 Cell culture

This section will introduce the methods and techniques used for culturing cells before and after bioprinting. Both experimental situations require different methods to passage cells, which will be explained below. For the 3D cell culture systems, the use of a de-crosslinking agent sodium citrate (55 mM) is required to digest the bioprinted ECM analog, while the 2D cell culture requires trypsin-EDTA to disrupt cell attachments to the bottom of the dish. For this project, we report the use of two immortalized cell lines from human adenocarcinomas: MDA-MB-231-GFP and MCF-7. Both were cultured in 2D conditions before creating the cell-laden bioinks and scaffolds. For 2D and 3D conditions, the following medium composition was used: DMEM medium (Gibco, pH 7.2) supplemented with 10% fetal bovine serum (Wisent Bioproducts) and 1% v/v of streptomycin (Sigma-Aldrich). Cells were counted by using an automated cell counter (Invitrogen). Six samples of crosslinked cell-free (non-printed) bioink were placed on a culture dish inside the incubator (5% CO_2) for 48 h to discard any biological contaminations. Bacteria formation would be easily identified by optical microscopy due to a darker coloration of the scaffolds as well as the reaction with the buffer in the media. The following sections are ordered as if the user intended to perform the bioprinting process of a cell line.

2.6 Two-dimensional cell culture

Cells were cultured using traditional procedures: monolayer cultures were grown on T-75 flasks and passaged with trypsin-EDTA (0.25%-1X, Gibco) when 80% of cellular confluence was reached. Cell culture media was replaced every third day. After thawing frozen vials, cells had to be passaged at least 4 times to stabilize their metabolic activity before creating cell-laden scaffolds.

2.7 Scaffold design and 3D bioprinting

We designed the 3D scaffolds as disks with the following characteristics: 4 mm in diameter and 600 ± 50 µm in thickness; 4 layers per model. The code of the bioprinted model was written on a text file using G-code format. Lattices were bioprinted using a BioScaffolder 3.1 extrusion bioprinter (GeSiM, Germany). The geometries were created by extruding concentric disks until the outer diameter was reached. By choosing this geometry, we maintain a high-throughput production line with a post-printing sample validation under a light microscope.

Before starting, the bioink material was heated in a water bath (37 °C) for 30 min. Cells cultured in 2D conditions were harvested using trypsin-EDTA (see section 2.6). $1x10^6$ cells were isolated and placed in an Eppendorf tube and centrifuged at 1000 rpm for 5 min. The supernatant was removed and replaced by 50 µL of DMEM. The cell pellet was dissociated by micropipetting considering 50 µL for every mL of bioink. The liquid bioink was loaded into a printing cartridge, and the cells were mechanically mixed with a spatula. The cell-laden bioink was then centrifuged to get rid of the bubbles generated by the mixing procedure. The material was left for sol-gel transition: the bioink should reach its

optimal printing conditions 20 min after it was initially removed from the water bath. The models were printed using a 25-gauge conical nozzle. Right after printing, each sample was soaked in a solution of $CaCl_2$ (100 mM) for 1 min, rinsed twice with DPBS 1x, and placed in their final culture dish for cell culture (see section 2.8 for more details on the 3D cell culture method). Optical assessment of the models was performed, and the irregularities were isolated on a separate culture plate.

Our proposed geometry yielded 45 to 60 bioprinted samples that can be produced out of 1 mL of cell-laden A1G7 bioink. The whole bioprinting process took 60 min to complete. Depending on the cell type and the duration of the extrusion process, cell viability and post-printing behavior could be compromised.

2.8 Three-dimensional cell culture

After 3D bioprinting, cell-laden scaffolds were rinsed twice with DPBS before placing them in 3 cm (diameter) agarose-coated culture dishes to avoid cell attachment to the bottom. A maximum of 10 and a minimum of 3 bioprinted models placed per culture dish, this number could be upscaled or downscaled by considering the size of the culture dish. Once in their final culture dish, fresh media was added and replaced every 3 days. Samples were placed on new agarose-coated dishes every 3 days, and 3D cell passaging was conducted after 21 days of culture.

2.9 Three-dimensional cell passaging

Bioprinted scaffolds were placed on centrifuge tubes containing sodium citrate (55 mM) solution (55 mM, 37 °C). For the bioprinted structures of this project, 3 mL of sodium citrate were considered for every 10 scaffolds. Mechanical disruption of the matrix was

facilitated by using a vortex mixer (300 rpm) during the digestion process. 7 mL of DMEM at 37 °C were gently added into the tube to reduce osmotic shock. The contents of the tube were centrifuged at 700 rpm for 5 min. The supernatant was removed and replaced by 1 mL of trypsin-EDTA *(*0.25%-1X) and the solution was mechanically agitated by a vortex mixer (300 rpm) and several micropipetting steps to dissociate the MCTSs by disrupting cell-cell interactions by enzymatic digestion. 7 mL of DMEM at 37 °C were slowly added to stop the enzymatic effects of trypsin-EDTA and the cell suspension was centrifuged for 5 min at 1000 rpm and finally resuspended in 1 mL of DMEM. A light microscope was used to confirm spheroid dissociation into single cells, and the cell density was adjusted to $1x10^6$ cells/mL by an automated cell counter. Cells where then ready to be loaded into the bioink material for bioprinting again.

The procedure can be terminated after the spheroid release or the cell release steps to perform specific studies on either of the structures.

2.10 Histological sample preparation

Bioprinted samples were rinsed twice with DPBS and fixed with ice-cold 4% paraformaldehyde for 2 h. Increasing concentrations of ethanol (25%, 50%, 70%, and 95%) were used to dehydrate the samples, each solution was applied to the sample for 10 min. Absolute ethanol (95%) washes were repeated three times followed by three xylene washes. Finally, the samples we immersed in paraffin wax for 1 h (twice). Sections of 4-8 mm were obtained using a microtome. Eosin and hematoxilyn stainings (H&E, Leica ST Infinity H&E stain) were applied using Leica® TS5025 specimen stainer.

2.11 Confocal microscopy

Sample imaging was done using a confocal spinning disk inverted microscope Olympus IX83 (Olympus Life Science) considering a step size of 5 μm and an objective lens 10X/0.40na, 3.1mm working distance (UPlanSApo Olympus). For imaging studies on the confocal microscope, four samples were randomly selected from a sample pool of 20 and were imaged inside sterile containers at room temperature (24 °C). Image stacking and analysis was performed by Image J software.

2.12 Software and statistical analysis

Segmentation tools from ImageJ were used to obtain data on the cellular kinetics from the histology samples and the confocal images. Statistical analyses and graphs were conducted with GraphPad Prism 7 and Origin Pro®9. One Way ANOVA tests considered >100 samples per group (unless otherwise specified). MATLAB fitting tools (cftool) were used to study the growth kinetics (doubling time) of the geometric mean values of the samples.

3 Results

3.1 Physico-chemical characterization

In Figure 3-1, the FTIR spectra reveal the characteristic fingerprint for alginate around 946 cm^{-1}; attributed to 1→4 linkage between D-mannuronic acid and L-guluronic acid residues. Furthermore, alginate spectral bands at 904 cm^{-1} and 811 cm^{-1} are attributed to the C-H vibration of the saccharide ring of alginate (pyranose group)[120-122]. Gelatin spectra show characteristic bands at 1630 cm^{-1}, 1565 cm^{-1}, and 1240 cm^{-1} corresponding to amide-I, amide-II, and amide-III respectively[123].

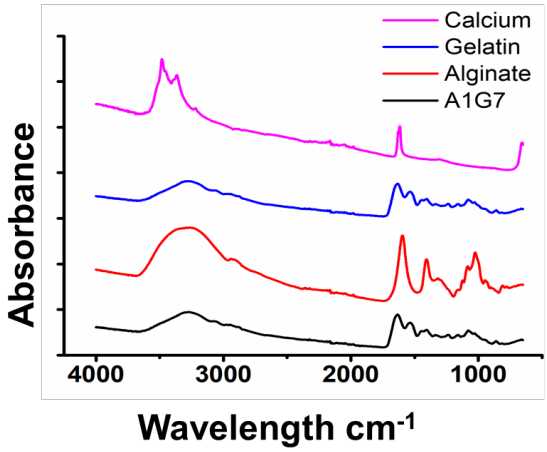

Gelatin	
Amide-I	1630 cm^{-1}
Amide-II	1565cm^{-1}
Amide-III	1240cm^{-1}
Alginate	
1→4 linkage between D-mannuronic and L-guluronic	946 cm^{-1}
C-H vibration of the saccharide ring of alginate	904 cm^{-1}
	811 cm^{-1}

Figure 3-1 Physico-chemical characterization. FTIR spectra of freeze-dried and crosslinked A1G7 (black line), powder alginate (red line), powder gelatin (blue line), a calcium powder (magenta line).

Furthermore, the liquid form of the bioink (37 °C), shown in Figure 3-2.b, is optimal for mixing live cells before the extrusion process. Gelation kinetics of the A1G7 precursor shows an increase of G' and G''at the sol-gel transition at 25 °C after approximately 5 min (Figure 3-2.a) of being exposed to room temperature. In practice, the bioprinting window of A1G7 precursor is reached after 25 min, requiring a constant pressure of 55 ± 5 kPa to extrude it during the bioprinting process. It is worth noting that the practical bioprinting window will always be different from the theoretical one; the experimental

conditions do not simulate complex variables such as temperature diffusion across irregular shapes and different materials and bioink dehydration during extrusion.

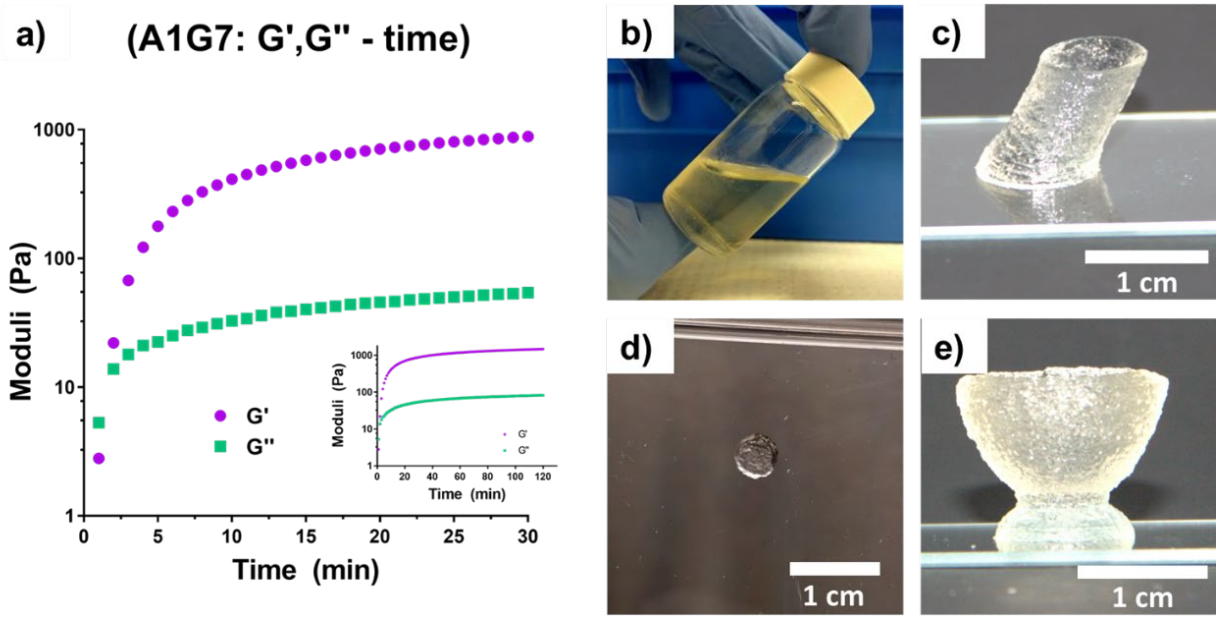

Figure 3-2 Physico-chemical characterization. a) Gelation kinetics of A1G7 hydrogel precursor. b) A1G7 bioink precursor in its liquid form at 37 °C. c) Bioprinted angled tube. d) Disk model for 3D cell culture. e) Bioprinted wine glass.

The bioink precursor will remain extrudable during the bioprinting window, which we tested for up to 2 h (Figure 3-2.a) inset). Moreover, current investigations in our laboratory (unpublished work, Jiang, 2018) concluded that Young's modulus of crosslinked A1G7 bioink is in the range of 5-9 kPa. Also, Figure 3-2.d shows the bioprinted disk model (cell-free), Figure 3-2.c and Figure 3-2.e show bioprinted, uncrosslinked A1G7 structures that can maintain their structural integrity after the extrusion process. These scaffolds were printed to assess the printability of our bioink qualitatively.

3.2 Three-Dimensional Cancer Cell Culture

Cells within the bioprinted scaffolds proliferated and reorganized into multicellular tumor spheroid (MCTSs). 2D and 3D cell morphologies are shown in Figure 3-3.

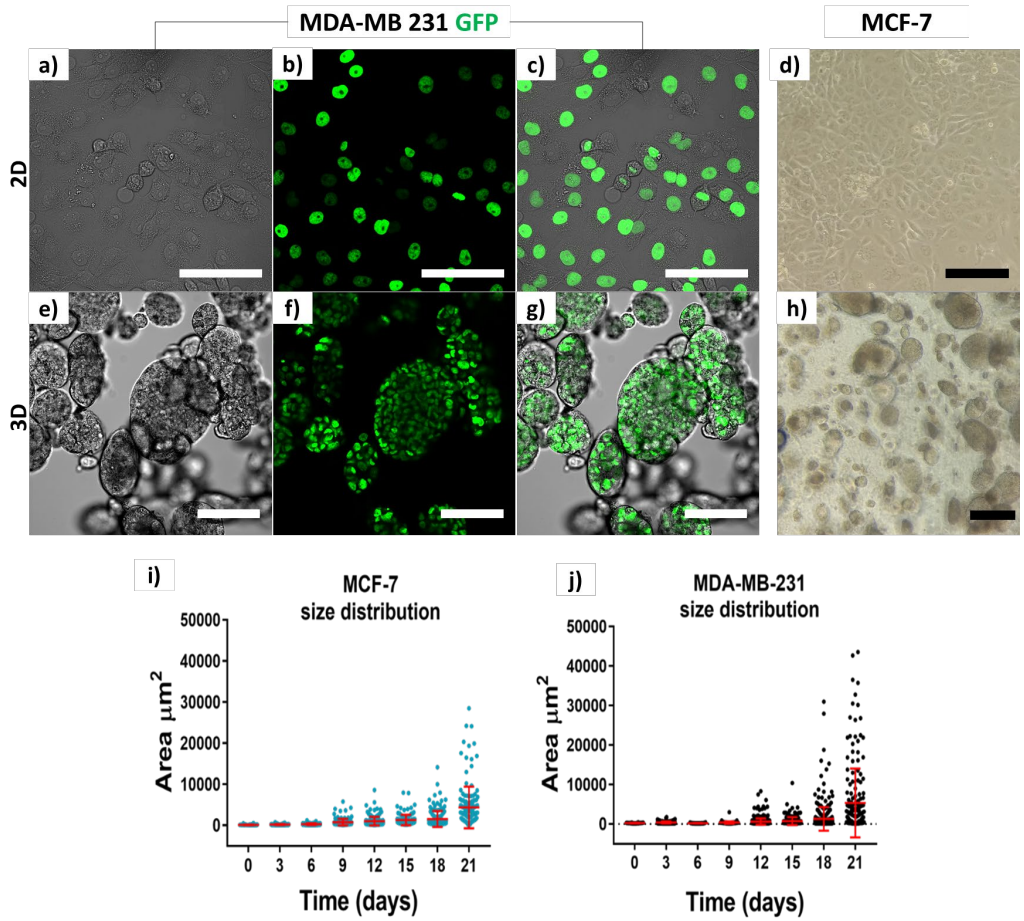

Figure 3-3 Cell morphology in 2D and 3D. MDA-MB-231-GFP (nuclear GFP) and MCF-7 cell lines were imaged after 24 h for 2D and after 21 days for 3D. Scale bars = 100 µm. Spheroid size distribution vs. time. i) MDA-MB-231. j) MCF-7. Mean values and standard deviation used as error. a), b), and c) were imaged by using phase contrast. e), f), and g) were imaged by getting a z-stack of MDA-MB-231-GFP MCTSs formations while floating in suspension. d) and h) panel were obtained by phase contrast microscopy of the cell monolayer and MCTSs inside A1G7.

Furthermore, our results (Figure 3-3.i and .j) show non-uniform spheroid size populations within the bioprinted samples for both MDA-MB-231 and MCF-7 cell lines. Analyses on cell distribution and growth kinetics are shown in Figure 3-5. Panels a) and c) show the qualitative overview of the MCTSs formation. Panels b) and d) represent the percentage of MCTSs distribution as a function of time. MCTSs were classified into the three area categories shown in Table 6 to perform growth kinetic studies.

Table 6 Area categories for growth kinetic analysis from histology data.

Cell type	Small (μm^2)	Medium (μm^2)	Large (μm^2)
MCF-7	50-1000	1001-2000	<2000
MDA-MB-231	180-2000	2001-4000	<4001

These data reveal that single cells and small spheroids tend to reduce in numbers while medium and big spheroids increase; an observation that supports the idea that cells proliferate, and spheroids grow over time. Doubling times of 110 h for MCF-7 and 116 h MDA-MB-231 respectively (~ 5 days), were obtained by using the model of exponential growth (Equation 3-1) and computed as Equation 3-2.

Equation 3-1

$$Y = Y_0 e^{k*t}$$

Equation 3-2

$$t = \frac{\ln(2)}{k}.$$

Data for exponential model was computed from the geometric mean (GM) of the distributions shown in Figure 3-5.f. Y0 is the value at time zero. k is the rate constant. Tau is the time constant, expressed in the same units as the X axis and it is computed as the reciprocal of k.

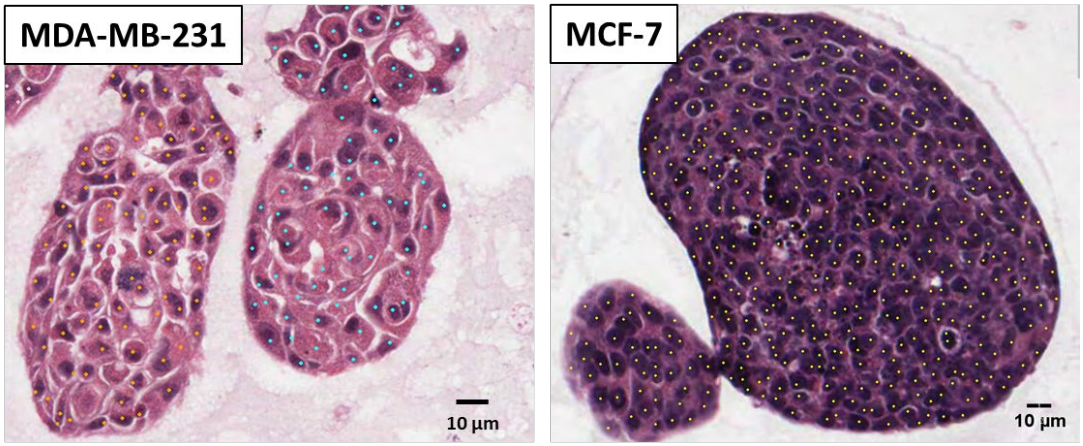

Figure 3-4 Multicellular tumor spheroids of MDA-MB-231 and MCF-7 processed by histology and stained with H&E. Sample images used for cell size quantifications. Cell nuclei were manually identified within the MCTSs structures. Cell area calculations were performed every 3 days. Spheroid formations correspond to 21 days in culture inside the ECM analog A1G7.

The minimum value of the small spheroids was considered as the area occupied by a single cell. Our measured cross-sectional area of a single MDA-MB-231 cell was 190 ± 10 μm^2, while each MCF-7 cell measured 51 ± 2 μm^2. Figure 3-4 shows spheroid morphologies and internal cell reorganization. The dots inside the spheroids correspond to the cell nuclei.

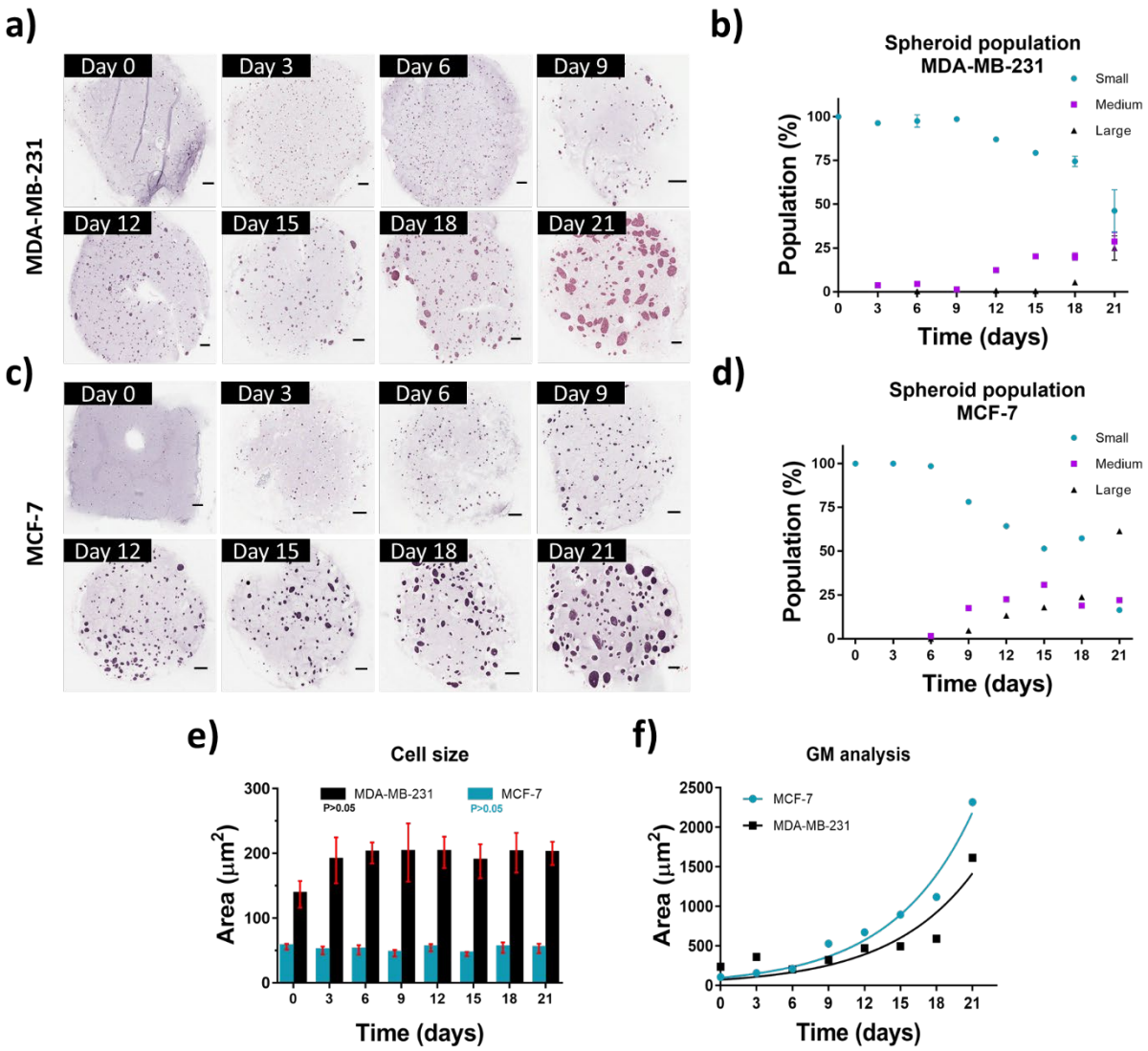

Figure 3-5 Growth kinetics and cell size analysis. a) MDA-MB-231 and c) MCF-7 timeline analyses of bioprinted samples processed by histology and stained with H&E. Slide thickness = 8 µm. Scale bars = 200 µm. b) MDA-MB-231 and d) MCF-7 MCTS population fractions throughout time. e) Cell size. f) Geometric mean (GM) analysis using Equation 3-1; values of MCTSs area distributions (R^2 for MCF is 0.96 and for MDA-MB-231 R^2 is 0.82). MDA-MB-231 growth kinetics results are also presented in Figure 3-8.

We studied our MCTS populations by using the GM because unlike the arithmetic mean, the GM represents the central value of a distribution and does not get drastically affected by large values or outliers present in skewed distributions (Figure 3-3.i and .j)[124,125].

3.3 Three-dimensional cell passaging

3D cell passaging involved an initial bioprinting procedure starting from a cell monolayer (Figure 3-6.a and .b), followed by a period of cell culture (Figure 3-6.c). When the desired time had been reached, MCTS formations were extracted from the matrix by a de-crosslinking procedure (Figure 3-6.d, .e and .f) using a $CaCl_2$ solution. At this point, spheroids were released (Figure 3-6.j) for dissociation by trypsinization and passage by reprinting (Figure 3-6.g, .h and .b).

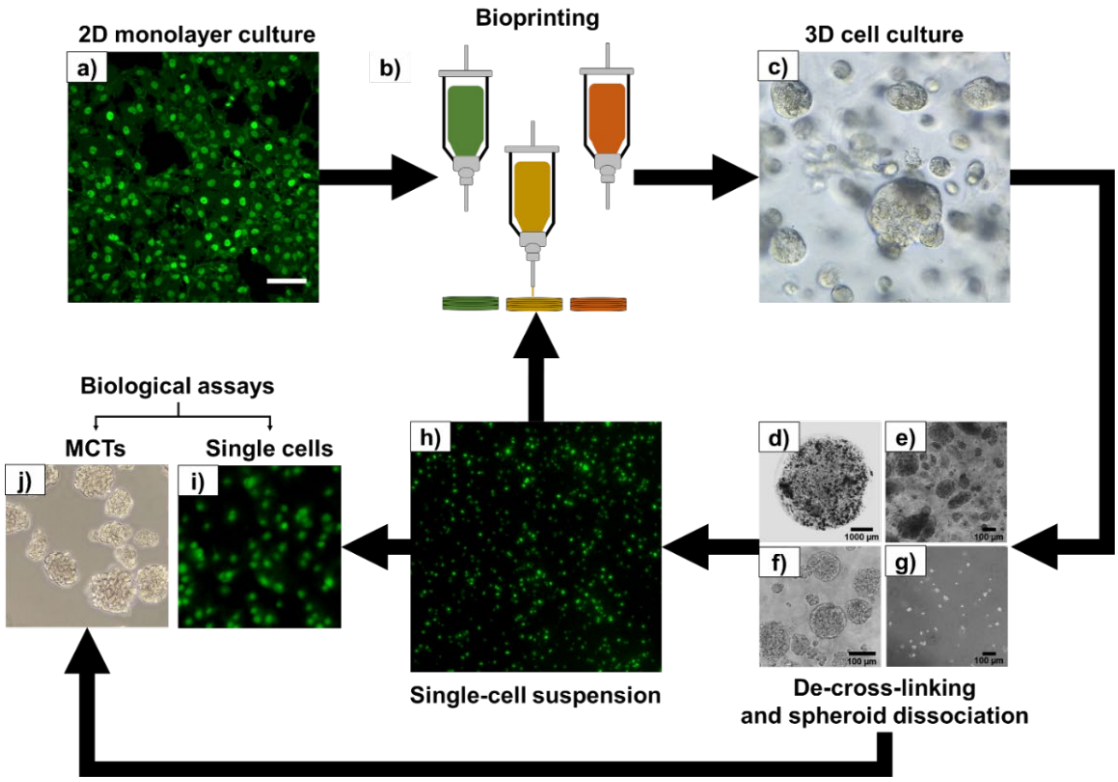

Figure 3-6 Three-dimensional cell passaging with bioprinting. a) 2D monolayer cell culture scale bar = 50 µm. b) Bioprinting cartoon c) MCTSs cultured inside A1G7 for 21 days. Phase contrast microscopy. d) Bioprinted disk model laden with cancer cells. Image by light microscopy. e) MCTSs inside A1G7 after 21 days of culture. f) MCTSs release by matrix disruption by de-crosslinking agents ($CaCl_2$, 100mM). g) MCTSs dissociation by trypsinization. h) Single-cell suspension ready for reprinting. i) and j) Single cells and MCTSs for biological assays.

Among our observations, MCTSs of MCF-7 and MDA-MB-231 cells were seen in suspension, outside the A1G7 matrix, after 21 days in culture. The results of 3D cell

culture passages are shown in Figure 3-7. We used MDA-MB-231-GFP breast cancer cells, and these were passaged after 21 days of culture. Our microscopy observations reveal a consistent growth behavior during 3D cell passages (81 days of culture). Single cells (day 0) reorganized into MCTSs when cultured for the 3 implemented passages.

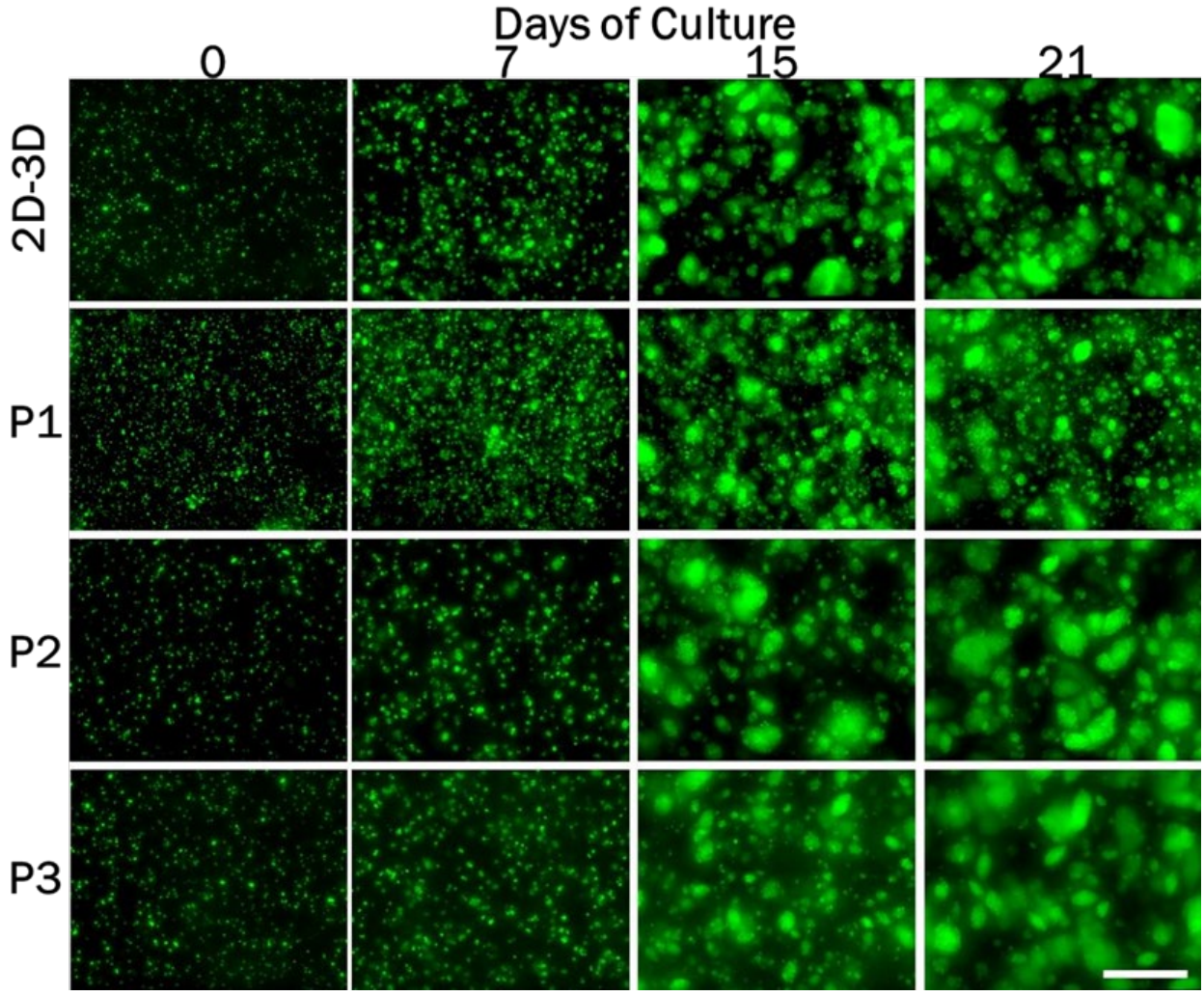

Figure 3-7 Three-dimensional cell culture with bioprinting techniques. MDA-MB-231-GFP breast cancer cells. Maximum intensity projection of Z stacks obtained by confocal microscopy. 2D-3D bioprinting is considered to be passage 0. Following 3D passages are described as P1, P2, and P3. Scale bar = 500 µm.

During our experimental setup and analyses, we found out that significant differences are the result of inconsistent MCTSs dissociation (trypsinization step). Furthermore, ANOVA tests conducted on the quadruplicate samples of each day revealed statistical similarities

on each sample. Again, the geometric mean (GM) values were computed and fitted into exponential growth equations to account for outliers in our data sets. Figure 3-8 shows the GM analysis of the 3D cell passaging. The GM values for MDA-MB-231 cell line growth kinetics were fitted to exponential equation (Equation 3-1).

Exponential growth model $Y = Y_0 e^{k*t}$				
3D passage number	**Y0**	**k**	**Doubling time (days)**	r^2
0	178.3	0.1598	4.34	**0.9939**
1	186.6	0.1457	4.76	**0.9979**
2	547	0.13	5.368	**0.9929**
3	359	0.135	5.14	**0.9952**

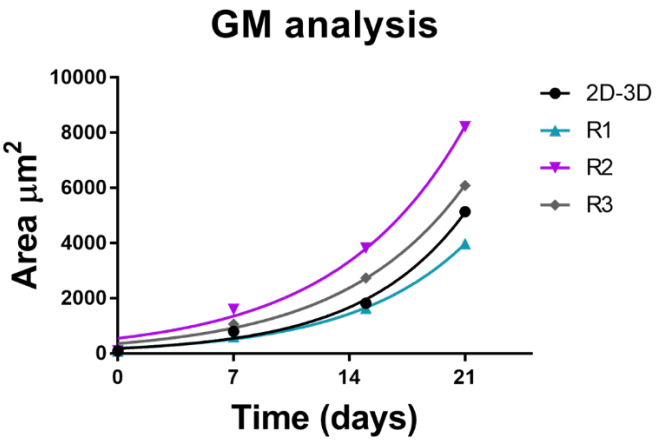

Figure 3-8 Geometric mean analysis of three-dimensional passages of MDA-MB-231. Y0 is the value at time zero. k is the rate constant. Tau is the time constant, expressed in the same units as the X axis. Computed as the reciprocal of k. The doubling time is in the time units of the X axis, computed as ln(2)/k.

Also, doubling times were computed for MDA-MB-231 MCTSs. Our results indicate that each passage exhibits a doubling time between 4 to 5 days, which is in good concordance to the approximated doubling time obtained by the histology data (110 h or 4.6 days). The results from different experimental approaches indicate that the time it takes for the MDA-MB-231 MCTS population to double its size is 4.8 ± 0.4 days.

4 Discussion

Alginate and gelatin are naturally derived materials often prepared as hydrogel precursors in tissue engineering applications. These precursors are used as bioinks in 3D bioprinting due to their biological and physical attributes. The gelatin concentration influences the bioprinting window of these composite hydrogel precursors. The time to reach the bioprinting window can be shortened or lengthened by either reducing or increasing the gelatin concentration. The alginate concentration is known to be directly proportional to the modulus of the hydrogel precursor. The emulation of soft or stiff ECM can be achieved by increasing or reducing the alginate and cross-linker concentration[126]. However, these variations may not be suitable for every cell type. Increasing alginate concentrations have been related to morphological cell changes and cell behavior in 3D cell cultures[127].

The effects of ECM stiffness on the TME been extensively documented on 2D and 3D cell culture systems. In 2D models, cells are placed on top of a coated surface (usually collagen or fibronectin) while the 3D systems use either single cells or MCTSs embedded in gels or hydrogels. In both cases, stiffness can be increased by modifying the protein concentration or the degree of crosslinking of the matrix. Stiffer substrates and matrices have been linked to activation of intracellular signaling that regulates cancer-associated genes, favoring cell survival, migration, and invasion[128,129]. For example, it was reported that tissue stiffness activates transcription factor TWIST1 in breast cancer cells, which inhibits the production of the cell-cell adhesion molecule E-cadherin, resulting in cancer metastasis and invasion. Some other studies conclude that cancer cells exhibit higher viability developing in soft hydrogel environments[130].

Even though alginate is the major contributor to microenvironmental stiffness post-printing, it remains as a bioinert biomaterial. The gelatin component of the composite hydrogel bioink accounts for the yield stress of the material during the scaffolding process. Partial structure recovery of the triple helix of collagen occurs frequently enough to give the precursor sufficient yield strength to be extruded without flowing. Furthermore, the gelatin component plays another critical role in enhancing the bioactivity of the bioink. Cell binding sequences of Arg-Gly-Asp (RGD) can be identified by integrins (cell adhesion molecules). The presence of integrin binding allows cells to respond to the microenvironment by using these transmembrane proteins[131]. Biocompatibility on hydrogel materials can be enhanced by adding gelatin[132]. Gelatin concentration has been related to morphological cell changes and proliferation rates[133].

Gelatin and alginate concentrations are essential variables to consider in the final microenvironment as different cell types may benefit from ECM analogs with specific mechanical and bioactive properties. Our bioink formulation (A1G7) allowed single cells to reorganize into multicellular tumor spheroids (MCTSs) during culture conditions. For both cell lines (MDA-231 and MCF-7) small MCTS start forming after 6 days of culture (histology panel in Figure 3-5) and these multicellular structures will continue to grow over time. Large MCTSs started to exit the ECM analog after 21 days of culture. This could be attributed to alginate-gelatin matrix degradation and possible migration events throughout the culture time[72,134]. Further data acquisition after 21 days of culture could jeopardize the reproducibility of our observations due to the uncontrolled evacuation of MCTSs.

Many researchers have reported several methods for MCTSs formation: floating on non-adhesive surfaces[135,136], hanging drop[137,138], spinner inside the culture vessel, rotation of the culture vessel[139], magnetic levitation[140,141], microfluidic devices[142], gel embedding[143], and 3D scaffolding[72]. Our method for MCTS formation relies on the ability of cells to self-assembly. Our datasets revealed that 3D long-term cell culture (~ 80 days) is possible and it suggests that cell viability is not compromised during the printing process due to subsequent cellular reorganization into MCTSs. By implementing the reprinting procedures, the control of the microenvironment allowed reproducible results regarding MCTSs formation and development over time.

When cultured in 2D conditions, MCF-7 and MDA-MB-231 require 1 to 1.5 days for the cell population to double[144,145]. In our alginate-gelatin cell culture systems, MCTSs doubled in size after 4 to 5 days of culture. The difference in cell division rates may be attributed to the disposition of nutrients and the presence of a porous, stiff matrix that promotes cell-cell and cell-ECM interactions. For 3D cancer cell culture, it has been documented that necrotic cores within the MCTSs are the result of nutrient, oxygen, and waste gradients. In 2D systems, cells are abnormally grown on a flat, rigid surface. Cells under these conditions are equally exposed to the nutrient source and rarely exhibit cell necrosis or apoptosis if cultured under appropriate conditions[146].

Proliferation rates of cells in 3D environments may also be altered by the stimuli from the ECM and surrounding cells that activate molecular signaling of dwelling cells. It has been reported that colonospheres (colorectal cancer spheroids) showed reduced proliferative rates compared to their monolayer equivalents[147].

Our histologial results revealed morphological differences betweenf MDA-MB-231 and MCF-7 MCTSs. MCF-7 cells were consistently found tightly packed in the spheroid formations compared to MDA-MB-231 cell reorganization (Figure 3-4). These observations could be attributed to adhesion molecules expressed by both cell lines while cultured in 3D conditions. MCF-7 are known to express E-cadherin and in greater quantities than β1-integrins, as revealed by western blot analysis. E-cadherin is responsible for cell-cell attachments[148] while β1-integrin modulates cell-ECM interactions[149]. The ratio of these molecules on the surface of MCF-7 cells could explain the morphology of cell reorganization into tight structures since MCF-7 are expected to favor cell-cell interactions. On the other hand, western blot analysis revaled that MDA-MB-231 cells only expressed β1-integrin[150]. We believe that the lack E-cadherin results in loose cell-cell junctions within the MDA-MB-231 MCTSs.

Intrinsic cellular functions such as proliferation rates and differentiation can be altered by inappropriate cell culture conditions[151]. The reduced growth rates on 3D cell cultures alter the inhibitory activity of chemotherapeutical agents that target proliferative cells. 3D culture systems allow intermolecular cell dialogue and cell-ECM interactions. The effects of anti-proliferative drugs on 2D cultures are considerably different from than those for cells cultured inside an ECM analog[152]. Cell-ECM interactions have been related to enhanced cell survival and therapy resistance[153].

Our 3D cell passaging procedures allowed us to restart the culture conditions from single cells after 21 days. We successfully passaged 3 times and stopped the experiment after

84 days of culture (Figure 3-6). The MDA-MB-231-GFP cell line showed a consistent pattern of reproduction rates and morphological reorganization during the experiment.

Overall cancer spheroid models have been a useful tool to study malignant neoplasms. The MCTSs model has been widely used in the screening of chemotherapeutical agents since the model emulates fundamental characteristics of the TME in which cancer cells live[154]. Our 3D cell platform considers: (1) an ECM analog, capable of promoting cell dialog and cell-ECM interactions. (2) the cancer cells that reorganize into MCTSs over time.

5 Conclusions

In the present study, we showed that using extrusion bioprinting to control the TME initial conditions results in reproducible biological behaviors over time. Cancer cell reorganization produced relevant multicellular tumor structures with a vast number of applications in oncological and biomedical research. We proved that controlling the initial conditions of the 3D cell microenvironment allows reproducible results when culturing cell-laden scaffolds. Extrusion-based bioprinting was used in our study to perform 3D scaffolding of cancer cell-laden environments. We focused on characterizing the behavior of two breast cancer cell lines inside an alginate-gelatin ECM analog. Our 3D cell passaging method was improved using 3D bioprinting to ensure equal initial conditions for all the samples. Crosslinked A1G7 ECM analogs proved to be compatible with histological procedures and staining. MCTSs dissociation into single cells was accomplished by de-crosslinking agents. The use of bioprinting allowed us to perform 3D cell culture for extended periods of time (~ 80 days).

Overall, our studies on cell-laden scaffolds suggest that bioprinting technologies could improve current methodologies of high-throughput (HT) sample production. Availability of HT 3D sample production for HT drug screening would make a considerable impact in cancer research.

6 Future work

Future work for this project includes the exploration of druggable targets within the TME. Several research groups have suggested targeting ECM and the TME tissue and its molecular composition to limit pathological progression. For instance, targeting growth factors, such as TGFβ (transforming growth factor β), is an active research field for fibrosis and oncology. Extracellular TGFβ is known to induce collagen and fibronectin gene expression in myofibroblasts. Disrupting the role of TGFβ has been done by inhibiting receptor-ligand interactions, small-molecule inhibitors, and monoclonal antibodies[155]. Some other examples of growth factors implicated to fibrosis are platelet-derived growth factor (PDGF and vascular endothelial growth factor (VEGF). Both can be considered therapeutic targets[156,157]. Additional strategies include targeting cellular responses to increased ECM stiffness such as interrupting integrin binding and inhibiting Rho-associated kinase (ROCK) (which is a driver for cell contractility and mediator of fibrosis[158,159]) and targeting the enzyme lysyl oxidase (LOX) (known to remodel ECM thought oxidative processes)[160].

Further microscopy studies are proposed. Quantification of MCF-7 cell spheroid growth is required in order to complete the data set for the cell line. Cytoskeletal organization of actin filaments is also proposed to evaluate morphological differences between cell lines and their 2D cell culture counterparts. These analyses could offer insights on cytoskeletal reorganization during spheroid growth.

Immunohistochemistry of proliferation markers and caspase activity is also proposed to track necrotic core formation across time as well as cytochrome c analysis on the cytosol.

Genetic profiling of cell passages is considered in our future experiments since cells are known to undergo mutations during cell culture.

7 References

1 Committee, C. C. S. A. Canadian cancer statistics 2017. *Toronto, ON: Canadian Cancer Society* (2017).

2 Smith, H. S., Wolman, S. R. & Hackett, A. J. The biology of breast cancer at the cellular level. *Biochimica et biophysica acta* **738**, 103-123 (1984).

3 Hay, M., Thomas, D. W., Craighead, J. L., Economides, C. & Rosenthal, J. Clinical development success rates for investigational drugs. *Nature Biotechnology* **32**, 40, doi:10.1038/nbt.2786 (2014).

4 Barker, H. E., Paget, J. T. E., Khan, A. A. & Harrington, K. J. The Tumour Microenvironment after Radiotherapy: Mechanisms of Resistance and Recurrence. *Nature reviews. Cancer* **15**, 409-425, doi:10.1038/nrc3958 (2015).

5 Runa, F. *et al.* Tumor microenvironment heterogeneity: Challenges and opportunities. *Current molecular biology reports* **3**, 218-229 (2017).

6 Balkwill, F. R., Capasso, M. & Hagemann, T. The tumor microenvironment at a glance. *Journal of Cell Science* **125**, 5591-5596, doi:10.1242/jcs.116392 (2012).

7 Hanahan, D. & Coussens, Lisa M. Accessories to the Crime: Functions of Cells Recruited to the Tumor Microenvironment. *Cancer Cell* **21**, 309-322, doi: doi: 10.1016/j.ccr.2012.02.022 (2012).

8 Kalluri, R. & Zeisberg, M. Fibroblasts in cancer. *Nat Rev Cancer* **6**, 392-401, doi:10.1038/nrc1877 (2006).

9 Tomasek, J. J., Gabbiani, G., Hinz, B., Chaponnier, C. & Brown, R. A. Myofibroblasts and mechano-regulation of connective tissue remodelling. *Nature reviews. Molecular cell biology* **3**, 349-363, doi:10.1038/nrm809 (2002).

10 Xu, R., Boudreau, A. & Bissell, M. J. Tissue architecture and function: dynamic reciprocity via extra- and intra-cellular matrices. *Cancer metastasis reviews* **28**, 167-176, doi:10.1007/s10555-008-9178-z (2009).

11 Kim, Y., Ko, H., Kwon, I. K. & Shin, K. Extracellular Matrix Revisited: Roles in Tissue Engineering. *International Neurourology Journal* **20**, S23-29, doi:10.5213/inj.1632600.318 (2016).

12 Järveläinen, H., Sainio, A., Koulu, M., Wight, T. N. & Penttinen, R. Extracellular Matrix Molecules: Potential Targets in Pharmacotherapy. *Pharmacological Reviews* **61**, 198-223, doi:10.1124/pr.109.001289 (2009).

13 Bonnans, C., Chou, J. & Werb, Z. Remodelling the extracellular matrix in development and disease. *Nature reviews. Molecular cell biology* **15**, 786-801, doi:10.1038/nrm3904 (2014).

14 Rozario, T. & DeSimone, D. W. The extracellular matrix in development and morphogenesis: a dynamic view. *Developmental biology* **341**, 126-140, doi:10.1016/j.ydbio.2009.10.026 (2010).

15 Maynes, R. *Structure and function of collagen types*. (Elsevier, 2012).

16 De Wever, O., Demetter, P., Mareel, M. & Bracke, M. Stromal myofibroblasts are drivers of invasive cancer growth. *International journal of cancer* **123**, 2229-2238, doi:10.1002/ijc.23925 (2008).

17 Kristensen, J. H. & Karsdal, M. A. in *Biochemistry of Collagens, Laminins and Elastin* (ed Morten A. Karsdal) 197-201 (Academic Press, 2016).

18 Cox, T. R. & Erler, J. T. Remodeling and homeostasis of the extracellular matrix: implications for fibrotic diseases and cancer. *Disease models & mechanisms* **4**, 165-178 (2011).

19 Erdogan, B. & Webb, D. J. Cancer-associated fibroblasts modulate growth factor signaling and extracellular matrix remodeling to regulate tumor metastasis. *Biochemical Society transactions* **45**, 229-236, doi:10.1042/BST20160387 (2017).

20 Hanahan, D. & Weinberg, R. A. The Hallmarks of Cancer. *Cell* **100**, 57-70, doi:doi: 10.1016/S0092-8674(00)81683-9 (2000).

21 Hanahan, D. & Weinberg, R. A. Hallmarks of cancer: the next generation. *Cell* **144**, 646-674, doi:10.1016/j.cell.2011.02.013 (2011).

22 Xing, Y., Zhao, S., Zhou, B. P. & Mi, J. Metabolic reprogramming of the tumour microenvironment. *The FEBS Journal* **282**, 3892-3898, doi:doi:10.1111/febs.13402 (2015).

23 Shu, H. & Li, H. F. Prognostic effect of stromal myofibroblasts in lung adenocarcinoma. *Neoplasma* **59**, 658-661, doi:10.4149/neo_2012_083 (2012).

24 Grotendorst, G. R., Rahmanie, H. & Duncan, M. R. Combinatorial signaling pathways determine fibroblast proliferation and myofibroblast differentiation. *FASEB journal : official publication of the Federation of American Societies for Experimental Biology* **18**, 469-479, doi:10.1096/fj.03-0699com (2004).

25 Gascard, P. & Tlsty, T. D. Carcinoma-associated fibroblasts: orchestrating the composition of malignancy. *Genes & development* **30**, 1002-1019, doi:10.1101/gad.279737.116 (2016).

26 LeBleu, V. S. & Kalluri, R. A peek into cancer-associated fibroblasts: origins, functions and translational impact. *Disease Models & Mechanisms* **11**, doi:10.1242/dmm.029447 (2018).

27 Orimo, A. *et al.* Stromal Fibroblasts Present in Invasive Human Breast Carcinomas Promote Tumor Growth and Angiogenesis through Elevated SDF-1/CXCL12 Secretion. *Cell* **121**, 335-348, doi:doi: 10.1016/j.cell.2005.02.034. (2005).

28 Jung, D.-W. *et al.* Tumor-stromal crosstalk in invasion of oral squamous cell carcinoma: a pivotal role of CCL7. *International journal of cancer* **127**, 332-344, doi:doi:10.1002/ijc.25060 (2010).

29 Zhuang, J. *et al.* TGFβ1 secreted by cancer-associated fibroblasts induces epithelial-mesenchymal transition of bladder cancer cells through lncRNA-ZEB2NAT. *Scientific Reports* **5**, 11924, doi:10.1038/srep11924 (2015).

30 Sun, Y. *et al.* Cancer-associated fibroblasts secrete FGF-1 to promote ovarian proliferation, migration, and invasion through the activation of FGF-1/FGFR4 signaling. *Tumor Biology* **39**, 1010428317712592, doi:10.1177/1010428317712592 (2017).

31 Ratajczak-Wielgomas, K. *et al.* Periostin expression in cancer-associated fibroblasts of invasive ductal breast carcinoma. *Oncology reports* **36**, 2745-2754 (2016).

32 Kalluri, R. The biology and function of fibroblasts in cancer. *Nature Reviews Cancer* **16**, 582, doi:10.1038/nrc.2016.73 (2016).

33 Kuzet, S.-E. & Gaggioli, C. Fibroblast activation in cancer: when seed fertilizes soil. *Cell and Tissue Research* **365**, 607-619, doi:10.1007/s00441-016-2467-x (2016).

34 Gascard, P. & Tlsty, T. D. Carcinoma-associated fibroblasts: orchestrating the composition of malignancy. *Genes & development* **30**, 1002-1019, doi:10.1101/gad.279737.116 (2016).

35 Utispan, K. *et al.* Gene expression profiling of cholangiocarcinoma-derived fibroblast reveals alterations related to tumor progression and indicates periostin as a poor prognostic marker. *Molecular Cancer* **9**, 13-13, doi:10.1186/1476-4598-9-13 (2010).

36 Liao, Z., Tan, Z. W., Zhu, P. & Tan, N. S. Cancer-associated fibroblasts in tumor microenvironment – Accomplices in tumor malignancy. *Cellular Immunology*, doi: doi: 10.1016/j.cellimm.2017.12.003 (2018).

37 Shiga, K. *et al.* Cancer-Associated Fibroblasts: Their Characteristics and Their Roles in Tumor Growth. *Cancers* **7**, 2443-2458, doi:10.3390/cancers7040902 (2015).

38 Lim, H. & Moon, A. Inflammatory fibroblasts in cancer. *Archives of Pharmacal Research* **39**, 1021-1031, doi:10.1007/s12272-016-0787-8 (2016).

39 Sugimoto, H., Mundel, T. M., Kieran, M. W. & Kalluri, R. Identification of fibroblast heterogeneity in the tumor microenvironment. *Cancer biology & therapy* **5**, 1640-1646 (2006).

40 Fu, Z. *et al.* The crosstalk: Tumor-infiltrating lymphocytes rich in regulatory T cells suppressed cancer-associated fibroblasts. *Acta Oncologica (Stockholm, Sweden)* **52**, 1760-1770, doi:10.3109/0284186X.2012.760847 (2013).

41 Wang, Y. *et al.* Cancer-associated Fibroblasts Promote Irradiated Cancer Cell Recovery Through Autophagy. *EBioMedicine* **17**, 45-56, doi:10.1016/j.ebiom.2017.02.019 (2017).

42 Shintani, Y. *et al.* IL-6 Secreted from Cancer-Associated Fibroblasts Mediates Chemoresistance in NSCLC by Increasing Epithelial-Mesenchymal Transition Signaling. *Journal of Thoracic Oncology* **11**, 1482-1492, doi:doi: 10.1016/j.jtho.2016.05.025 (2016).

43 Chaffer, C. L. & Weinberg, R. A. A perspective on cancer cell metastasis. *Science* **331**, 1559-1564, doi:10.1126/science.1203543 (2011).

44 Tarin, D. Cell and tissue interactions in carcinogenesis and metastasis and their clinical significance. *Seminars in cancer biology* **21**, 72-82, doi:10.1016/j.semcancer.2010.12.006 (2011).

45 Chambers, A. F., Groom, A. C. & MacDonald, I. C. Dissemination and growth of cancer cells in metastatic sites. *Nat Rev Cancer* **2**, 563-572, doi:10.1038/nrc865 (2002).

46 Fidler, I. J. The pathogenesis of cancer metastasis: the 'seed and soil' hypothesis revisited. *Nat Rev Cancer* **3**, 453-458, doi:10.1038/nrc1098 (2003).

47 Aravalli, R. N., Golzarian, J. & Cressman, E. N. K. Animal models of cancer in interventional radiology. *European Radiology* **19**, 1049-1053, doi:10.1007/s00330-008-1263-8 (2009).

48 Seyfried, T. *Cancer as a Metabolic Disease: On the Origin, Management, and Prevention of Cancer*. (Wiley, 2012).

49 Duan, B., Hockaday, L. A., Kang, K. H. & Butcher, J. T. 3D bioprinting of heterogeneous aortic valve conduits with alginate/gelatin hydrogels. *Journal of biomedical materials research Part A* **101**, 1255-1264 (2013).

50 Dai, X. *et al.* Coaxial 3D bioprinting of self-assembled multicellular heterogeneous tumor fibers. *Scientific reports* **7**, 1457 (2017).

51 Tekin, E., Smith, P. J. & Schubert, U. S. Inkjet printing as a deposition and patterning tool for polymers and inorganic particles. *Soft Matter* **4**, 703-713 (2008).

52 Olkkonen, J., Leppäniemi, J., Mattila, T. & Eiroma, K. Sintering of inkjet printed silver tracks with boiling salt water. *Journal of Materials Chemistry C* **2**, 3577-3582 (2014).

53 Villar, G., Graham, A. D. & Bayley, H. A tissue-like printed material. *Science* **340**, 48-52 (2013).

54 Xu, T., Jin, J., Gregory, C., Hickman, J. J. & Boland, T. Inkjet printing of viable mammalian cells. *Biomaterials* **26**, 93-99 (2005).

55 Orloff, N. D. *et al.* Integrated bioprinting and imaging for scalable, networkable desktop experimentation. *RSC Advances* **4**, 34721-34728 (2014).

56 Cui, X., Breitenkamp, K., Finn, M., Lotz, M. & D'Lima, D. D. Direct human cartilage repair using three-dimensional bioprinting technology. *Tissue Engineering Part A* **18**, 1304-1312 (2012).

57 Cui, X., Breitenkamp, K., Lotz, M. & D'Lima, D. Synergistic action of fibroblast growth factor-2 and transforming growth factor-beta1 enhances bioprinted human neocartilage formation. *Biotechnology and bioengineering* **109**, 2357-2368 (2012).

58 Cui, X., Gao, G. & Qiu, Y. Accelerated myotube formation using bioprinting technology for biosensor applications. *Biotechnology letters* **35**, 315-321 (2013).

59 Pepper, M. E. *et al.* in *Engineering in Medicine and Biology Society, EMBC, 2011 Annual International Conference of the IEEE.* 3609-3612 (IEEE).

60 Pepper, M. E., Seshadri, V., Burg, T. C., Burg, K. J. & Groff, R. E. Characterizing the effects of cell settling on bioprinter output. *Biofabrication* **4**, 011001 (2012).

61 Lee, W. *et al.* Multi-layered culture of human skin fibroblasts and keratinocytes through three-dimensional freeform fabrication. *Biomaterials* **30**, 1587-1595 (2009).

62 Zhang, A. P. *et al.* Rapid fabrication of complex 3D extracellular microenvironments by dynamic optical projection stereolithography. *Advanced materials* **24**, 4266-4270 (2012).

63 Lin, H. *et al.* Application of visible light-based projection stereolithography for live cell-scaffold fabrication with designed architecture. *Biomaterials* **34**, 331-339 (2013).

64 Lee, S.-J., Rhie, J.-W. & Cho, D.-W. Development of three-dimensional alginate encapsulated chondrocyte hybrid scaffold using microstereolithography. *Journal of Manufacturing Science and Engineering* **130**, 021007 (2008).

65 Lee, S.-J. *et al.* Application of microstereolithography in the development of three-dimensional cartilage regeneration scaffolds. *Biomedical microdevices* **10**, 233-241 (2008).

66 Moan, J. & Peak, M. J. Effects of UV radiation on cells. *Journal of Photochemistry and Photobiology B: Biology* **4**, 21-34, doi:doi: 10.1016/1011-1344(89)80099-5 (1989).

67 Hopp, B. *et al.* Survival and proliferative ability of various living cell types after laser-induced forward transfer. *Tissue engineering* **11**, 1817-1823 (2005).

68 Koch, L. *et al.* Laser printing of skin cells and human stem cells. *Tissue Engineering Part C: Methods* **16**, 847-854 (2009).

69 Guillotin, B. *et al.* Laser assisted bioprinting of engineered tissue with high cell density and microscale organization. *Biomaterials* **31**, 7250-7256 (2010).

70 Murphy, S. V. & Atala, A. 3D bioprinting of tissues and organs. *Nature biotechnology* **32**, 773 (2014).

71 Guillotin, B. & Guillemot, F. Cell patterning technologies for organotypic tissue fabrication. *Trends in biotechnology* **29**, 183-190 (2011).

72 Jiang, T. *et al.* Directing the self-assembly of tumour spheroids by bioprinting cellular heterogeneous models within alginate/gelatin hydrogels. *Scientific Reports* **7**, 4575 (2017).

73 He, Y. *et al.* Research on the printability of hydrogels in 3D bioprinting. *Scientific reports* **6**, 29977 (2016).

74 Tabriz, A. G., Hermida, M. A., Leslie, N. R. & Shu, W. Three-dimensional bioprinting of complex cell laden alginate hydrogel structures. *Biofabrication* **7**, 045012 (2015).

75 Di Giuseppe, M. *et al.* Mechanical behaviour of alginate-gelatin hydrogels for 3D bioprinting. *Journal of the mechanical behavior of biomedical materials* **79**, 150-157 (2018).

76 Webb, B. & Doyle, B. J. Parameter optimization for 3D bioprinting of hydrogels. *Bioprinting* **8**, 8-12 (2017).

77 Nair, K. *et al.* Characterization of cell viability during bioprinting processes. *Biotechnology Journal: Healthcare Nutrition Technology* **4**, 1168-1177 (2009).

78 Blaeser, A. *et al.* Controlling shear stress in 3D bioprinting is a key factor to balance printing resolution and stem cell integrity. *Advanced healthcare materials* **5**, 326-333 (2016).

79 Chang, R., Nam, J. & Sun, W. Effects of dispensing pressure and nozzle diameter on cell survival from solid freeform fabrication–based direct cell writing. *Tissue Engineering Part A* **14**, 41-48 (2008).

80 Ahlfeld, T. *et al.* Development of a clay based bioink for 3D cell printing for skeletal application. *Biofabrication* **9**, 034103 (2017).

81 Petersen, O. W., Rønnov-Jessen, L., Howlett, A. R. & Bissell, M. J. Interaction with basement membrane serves to rapidly distinguish growth and differentiation pattern of normal and malignant human breast epithelial cells. *Proceedings of the National Academy of Sciences* **89**, 9064-9068 (1992).

82 Liu, Z. & Vunjak-Novakovic, G. Modeling tumor microenvironments using custom-designed biomaterial scaffolds. *Current opinion in chemical engineering* **11**, 94-105 (2016).

83 Caliari, S. R. & Burdick, J. A. A practical guide to hydrogels for cell culture. *Nature methods* **13**, 405 (2016).

84 Hospodiuk, M., Dey, M., Sosnoski, D. & Ozbolat, I. T. The bioink: a comprehensive review on bioprintable materials. *Biotechnology advances* **35**, 217-239 (2017).

85 Pati, F. *et al.* Printing three-dimensional tissue analogues with decellularized extracellular matrix bioink. *Nature communications* **5**, 3935 (2014).

86 Hinderer, S., Layland, S. L. & Schenke-Layland, K. ECM and ECM-like materials—biomaterials for applications in regenerative medicine and cancer therapy. *Advanced drug delivery reviews* **97**, 260-269 (2016).

87 Tang, S., Yang, W. & Mao, X. Agarose/collagen composite scaffold as an anti-adhesive sheet. *Biomedical Materials* **2**, S129 (2007).

88 Livoti, C. M. & Morgan, J. R. Self-assembly and tissue fusion of toroid-shaped minimal building units. *Tissue engineering part A* **16**, 2051-2061 (2010).

89 Rowley, J. A., Madlambayan, G. & Mooney, D. J. Alginate hydrogels as synthetic extracellular matrix materials. *Biomaterials* **20**, 45-53 (1999).

90 Lee, K. Y. & Mooney, D. J. Alginate: properties and biomedical applications. *Progress in polymer science* **37**, 106-126, doi:10.1016/j.progpolymsci.2011.06.003 (2012).

91 Lotfipour, F., Mirzaeei, S. & Maghsoodi, M. Evaluation of the effect of CaCl2 and alginate concentrations and hardening time on the characteristics of Lactobacillus acidophilus loaded alginate beads using response surface analysis. *Advanced pharmaceutical bulletin* **2**, 71 (2012).

92 Croisier, F. & Jérôme, C. Chitosan-based biomaterials for tissue engineering. *European Polymer Journal* **49**, 780-792 (2013).

93 Geng, L. *et al.* Direct writing of chitosan scaffolds using a robotic system. *Rapid Prototyping Journal* **11**, 90-97 (2005).

94 Zhang, Y., Yu, Y. & Ozbolat, I. T. Direct bioprinting of vessel-like tubular microfluidic channels. *Journal of nanotechnology in engineering and medicine* **4**, 020902 (2013).

95 Ferreira, A. M., Gentile, P., Chiono, V. & Ciardelli, G. Collagen for bone tissue regeneration. *Acta biomaterialia* **8**, 3191-3200 (2012).

96 Themistocleous, G. *et al.* Three-dimensional type I collagen cell culture systems for the study of bone pathophysiology. *in vivo* **18**, 687-696 (2004).

97 Li, Y., Asadi, A., Monroe, M. R. & Douglas, E. P. pH effects on collagen fibrillogenesis in vitro: Electrostatic interactions and phosphate binding. *Materials Science and Engineering: C* **29**, 1643-1649 (2009).

98 Lam, J., Truong, N. F. & Segura, T. Design of cell–matrix interactions in hyaluronic acid hydrogel scaffolds. *Acta biomaterialia* **10**, 1571-1580 (2014).

99 Cui, X. & Boland, T. Human microvasculature fabrication using thermal inkjet printing technology. *Biomaterials* **30**, 6221-6227 (2009).

100 Gruene, M. *et al.* Laser printing of three-dimensional multicellular arrays for studies of cell–cell and cell–environment interactions. *Tissue Engineering Part C: Methods* **17**, 973-982 (2011).

101 Janmey, P. A., Winer, J. P. & Weisel, J. W. Fibrin gels and their clinical and bioengineering applications. *Journal of the Royal Society Interface* **6**, 1-10 (2009).

102 Sakai, S., Hirose, K., Taguchi, K., Ogushi, Y. & Kawakami, K. An injectable, in situ enzymatically gellable, gelatin derivative for drug delivery and tissue engineering. *Biomaterials* **30**, 3371-3377 (2009).

103 Benton, J. A., DeForest, C. A., Vivekanandan, V. & Anseth, K. S. Photocrosslinking of gelatin macromers to synthesize porous hydrogels that promote valvular interstitial cell function. *Tissue Engineering Part A* **15**, 3221-3230 (2009).

104 Nichol, J. W. *et al.* Cell-laden microengineered gelatin methacrylate hydrogels. *Biomaterials* **31**, 5536-5544 (2010).

105 Chiou, B.-S. *et al.* Cold water fish gelatin films: Effects of crosslinking on thermal, mechanical, barrier, and biodegradation properties. *European Polymer Journal* **44**, 3748-3753 (2008).

106 Kujawa, M. J. & Caplan, A. I. Hyaluronic acid bonded to cell-culture surfaces stimulates chondrogenesis in stage 24 limb mesenchyme cell cultures. *Developmental biology* **114**, 504-518 (1986).

107 Khattak, S. F., Bhatia, S. R. & Roberts, S. C. Pluronic F127 as a cell encapsulation material: utilization of membrane-stabilizing agents. *Tissue engineering* **11**, 974-983 (2005).

108 Gong, C. Y. *et al.* In vitro drug release behavior from a novel thermosensitive composite hydrogel based on Pluronic f127 and poly (ethylene glycol)-poly (ε-caprolactone)-poly (ethylene glycol) copolymer. *BMC biotechnology* **9**, 8 (2009).

109 Alconcel, S. N., Baas, A. S. & Maynard, H. D. FDA-approved poly (ethylene glycol)–protein conjugate drugs. *Polymer Chemistry* **2**, 1442-1448 (2011).

110 Vladkova, T., Krasteva, N., Kostadinova, A. & Altankov, G. Preparation of PEG-coated surfaces and a study for their interaction with living cells. *Journal of Biomaterials Science, Polymer Edition* **10**, 609-620 (1999).

111 Benoit, D. S., Durney, A. R. & Anseth, K. S. Manipulations in hydrogel degradation behavior enhance osteoblast function and mineralized tissue formation. *Tissue engineering* **12**, 1663-1673 (2006).

112 Mann, B. K., Gobin, A. S., Tsai, A. T., Schmedlen, R. H. & West, J. L. Smooth muscle cell growth in photopolymerized hydrogels with cell adhesive and proteolytically degradable domains: synthetic ECM analogs for tissue engineering. *Biomaterials* **22**, 3045-3051 (2001).

113 Ribeiro, M. *et al.* Development of silk fibroin/nanohydroxyapatite composite hydrogels for bone tissue engineering. *European Polymer Journal* **67**, 66-77 (2015).

114 Zhao, Y. *et al.* Three-dimensional printing of Hela cells for cervical tumor model in vitro. *Biofabrication* **6**, 035001 (2014).

115 Jia, J. *et al.* Engineering alginate as bioink for bioprinting. *Acta biomaterialia* **10**, 4323-4331 (2014).

116 Wu, Z. *et al.* Bioprinting three-dimensional cell-laden tissue constructs with controllable degradation. *Scientific reports* **6**, 24474 (2016).

117 Davidenko, N. *et al.* Evaluation of cell binding to collagen and gelatin: a study of the effect of 2D and 3D architecture and surface chemistry. *Journal of Materials Science: Materials in Medicine* **27**, 148 (2016).

118 Kalluri, R. The biology and function of fibroblasts in cancer. *Nature Reviews Cancer* **16**, 582 (2016).

119 Matsusaki, M. *et al.* Desmoplastic Reaction in 3D-Pancreatic Cancer Tissues Suppresses Molecular Permeability. *Advanced healthcare materials* **6**, 1700057 (2017).

120 Chandıa, N., Matsuhiro, B. & Vásquez, A. Alginic acids in Lessonia trabeculata: characterization by formic acid hydrolysis and FT-IR spectroscopy. *Carbohydrate Polymers* **46**, 81-87 (2001).

121 Bekhit, M., Sánchez-González, L., Messaoud, G. B. & Desobry, S. Design of microcapsules containing Lactococcus lactis subsp. lactis in alginate shell and xanthan gum with nutrients core. *LWT-Food Science and Technology* **68**, 446-453 (2016).

122 Lopes, S., Bueno, L., AGUIAR JÚNIOR, F. D. & Finkler, C. Preparation and characterization of alginate and gelatin microcapsules containing Lactobacillus rhamnosus. *Anais da Academia Brasileira de Ciências*, 0-0 (2017).

123 Das, M. P., R., S. P., Prasad, K., Jv, V. & M, R. EXTRACTION AND CHARACTERIZATION OF GELATIN: A FUNCTIONAL BIOPOLYMER. *2017*, 4, doi:10.22159/ijpps.2017v9i9.17618 (2017).

124 Alexander, N. Analysis of parasite and other skewed counts. *Tropical medicine & international health* **17**, 684-693 (2012).

125 Kirkwood, B. R. & Sterne, J. A. *Essential medical statistics*. (John Wiley & Sons, 2010).

126 Discher, D. E., Janmey, P. & Wang, Y.-l. Tissue cells feel and respond to the stiffness of their substrate. *Science* **310**, 1139-1143 (2005).

127 Shi, P., Laude, A. & Yeong, W. Y. Investigation of cell viability and morphology in 3D bio-printed alginate constructs with tunable stiffness. *Journal of Biomedical Materials Research Part A* **105**, 1009-1018 (2017).

128 Northey, J. J., Przybyla, L. & Weaver, V. M. Tissue force programs cell fate and tumor aggression. *Cancer discovery* (2017).

129 Gkretsi, V. & Stylianopoulos, T. Cell adhesion and matrix stiffness: coordinating cancer cell invasion and metastasis. *Frontiers in Oncology* **8**, 145 (2018).

130 Cavo, M. *et al.* Microenvironment complexity and matrix stiffness regulate breast cancer cell activity in a 3D in vitro model. *Scientific reports* **6**, 35367 (2016).

131 Nath, S. & Devi, G. R. Three-dimensional culture systems in cancer research: Focus on tumor spheroid model. *Pharmacology & therapeutics* **163**, 94-108 (2016).

132 Nieto-Suárez, M., López-Quintela, M. A. & Lazzari, M. Preparation and characterization of crosslinked chitosan/gelatin scaffolds by ice segregation induced self-assembly. *Carbohydrate polymers* **141**, 175-183 (2016).

133 Yang, G. *et al.* Enzymatically crosslinked gelatin hydrogel promotes the proliferation of adipose tissue-derived stromal cells. *PeerJ* **4**, e2497 (2016).

134 Li, Z. *et al.* Tuning Alginate-Gelatin Bioink Properties by Varying Solvent and Their Impact on Stem Cell Behavior. *Scientific reports* **8**, 8020 (2018).

135 Ivascu, A. & Kubbies, M. Rapid generation of single-tumor spheroids for high-throughput cell function and toxicity analysis. *Journal of biomolecular screening* **11**, 922-932, doi:10.1177/1087057106292763 (2006).

136 Ma, H. L. *et al.* Multicellular tumor spheroids as an in vivo-like tumor model for three-dimensional imaging of chemotherapeutic and nano material cellular penetration. *Molecular imaging* **11**, 487-498 (2012).

137 Kelm, J. M., Timmins, N. E., Brown, C. J., Fussenegger, M. & Nielsen, L. K. Method for generation of homogeneous multicellular tumor spheroids applicable to a wide variety of cell types. *Biotechnology and bioengineering* **83**, 173-180 (2003).

138 Oliveira, M. B. *et al.* Superhydrophobic chips for cell spheroids high-throughput generation and drug screening. *ACS applied materials & interfaces* **6**, 9488-9495, doi:10.1021/am5018607 (2014).

139 Ingram, M. *et al.* Three-dimensional growth patterns of various human tumor cell lines in simulated microgravity of a NASA bioreactor. *In vitro cellular & developmental biology. Animal* **33**, 459-466, doi:10.1007/s11626-997-0064-8 (1997).

140 Ino, K., Ito, A. & Honda, H. Cell patterning using magnetite nanoparticles and magnetic force. *Biotechnology and Bioengineering* **97**, 1309-1317 (2007).

141 Bae, J.-E. *et al.* The effect of static magnetic fields on the aggregation and cytotoxicity of magnetic nanoparticles. *Biomaterials* **32**, 9401-9414 (2011).

142 Moshksayan, K. *et al.* Spheroids-on-a-chip: Recent advances and design considerations in microfluidic platforms for spheroid formation and culture. *Sensors and Actuators B: Chemical* (2018).

143 Li, Y. & Kumacheva, E. Hydrogel microenvironments for cancer spheroid growth and drug screening. *Science advances* **4**, eaas8998 (2018).

144 Brinkley, B. *et al.* Variations in cell form and cytoskeleton in human breast carcinoma cells in vitro. *Cancer research* **40**, 3118-3129 (1980).

145 Sutherland, R. L., Hall, R. E. & Taylor, I. W. Cell proliferation kinetics of MCF-7 human mammary carcinoma cells in culture and effects of tamoxifen on exponentially growing and plateau-phase cells. *Cancer research* **43**, 3998-4006 (1983).

146 Gong, X. *et al.* Generation of multicellular tumor spheroids with microwell-based agarose scaffolds for drug testing. *PLoS One* **10**, e0130348 (2015).

147 Kanwar, S. S., Yu, Y., Nautiyal, J., Patel, B. B. & Majumdar, A. P. The Wnt/beta-catenin pathway regulates growth and maintenance of colonospheres. *Mol Cancer* **9**, 212, doi:10.1186/1476-4598-9-212 (2010).

148 Van Roy, F. & Berx, G. The cell-cell adhesion molecule E-cadherin. *Cellular and molecular life sciences* **65**, 3756-3788 (2008).

149 Wang, H., Luo, X. & Leighton, J. Extracellular matrix and integrins in embryonic stem cell differentiation. *Biochemistry insights* **8**, BCI. S30377 (2015).

150 Kenny, P. A. *et al.* The morphologies of breast cancer cell lines in three-dimensional assays correlate with their profiles of gene expression. *Molecular oncology* **1**, 84-96 (2007).

151 Benton, G., George, J., Kleinman, H. K. & Arnaoutova, I. P. Advancing science and technology via 3D culture on basement membrane matrix. *Journal of cellular physiology* **221**, 18-25, doi:10.1002/jcp.21832 (2009).

152 Lovitt, C. J., Shelper, T. B. & Avery, V. M. Doxorubicin resistance in breast cancer cells is mediated by extracellular matrix proteins. *BMC Cancer* **18**, 41, doi:10.1186/s12885-017-3953-6 (2018).

153 Lovitt, C. J., Shelper, T. B. & Avery, V. M. Doxorubicin resistance in breast cancer cells is mediated by extracellular matrix proteins. *BMC cancer* **18**, 41 (2018).

154 Chen, Y.-C., Lou, X., Zhang, Z., Ingram, P. & Yoon, E. High-throughput cancer cell sphere formation for characterizing the efficacy of photo dynamic therapy in 3D cell cultures. *Scientific reports* **5**, 12175 (2015).

155 Akhurst, R. J. & Hata, A. Targeting the TGFβ signalling pathway in disease. *Nature Reviews Drug Discovery* **11**, 790, doi:10.1038/nrd3810 (2012).

156 Heldin, C.-H. Targeting the PDGF Signaling Pathway in the Treatment of Non-Malignant Diseases. *Journal of Neuroimmune Pharmacology* **9**, 69-79, doi:10.1007/s11481-013-9484-2 (2014).

157 Schuppan, D. & Kim, Y. O. Evolving therapies for liver fibrosis. *The Journal of clinical investigation* **123**, 1887-1901, doi:10.1172/jci66028 (2013).

158 Street, C. A. & Bryan, B. A. Rho kinase proteins—pleiotropic modulators of cell survival and apoptosis. *Anticancer research* **31**, 3645-3657 (2011).

159 Htwe, S. S. *et al.* Role of Rho-associated coiled-coil forming kinase isoforms in regulation of stiffness-induced myofibroblast differentiation in lung fibrosis. *American journal of respiratory cell and molecular biology* **56**, 772-783 (2017).

160 Kagan, H. M. & Trackman, P. C. Properties and function of lysyl oxidase. *Am J Respir Cell Mol Biol* **5**, 206-210 (1991).